Understanding Terminal versus Bridging End-on N_2 Coordination in Transition Metal Complexes

Lynn S. Yamout,[1] Mohamad Ataya,[1] Faraj Hasanayn,[1,*] Patrick L. Holland,[2,*] Alexander J. M. Miller[3,*], and Alan S. Goldman[4,*]

[1] Department of Chemistry, *American University of Beirut*, Beirut 1107 2020, Lebanon

[2] Department of Chemistry, *Yale University*, New Haven, Connecticut 06520, United States

[3] Department of Chemistry, *University of North Carolina at Chapel Hill*, Chapel Hill, North Carolina 27599-3290, United States

[4] Department of Chemistry and Chemical Biology, *Rutgers, The State University of New Jersey*, New Brunswick, New Jersey 08903, United States

Corresponding Authors:

*E-mail: fh19@aub.edu.lb (F.H.)

*E-mail: patrick.holland@yale.edu (P.L.H.)

*E-mail: ajmm@email.unc.edu (A.J.M.M.)

*E-mail: alan.goldman@rutgers.edu (A.S.G.)

TOC Graphic

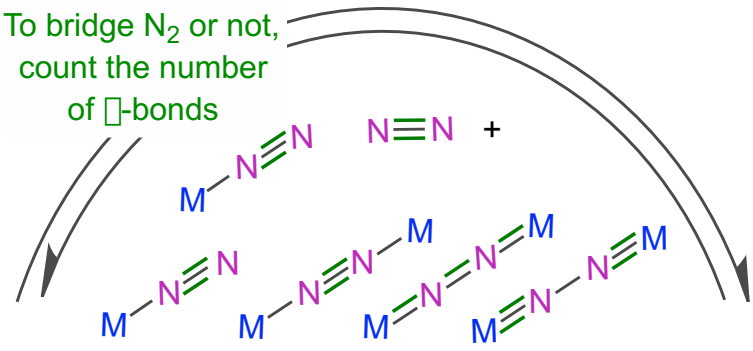

Abstract

Terminal and bridging end-on coordination of N_2 to transition metal complexes offer possibilities for distinct pathways in ammonia synthesis and N_2 functionalization. Here we elucidate the fundamental factors controlling the two binding modes and determining which is favored for a given metal-ligand system, using both quantitative density functional theory (DFT) and qualitative molecular orbital (MO) analyses. The Gibbs free energy for converting two terminal MN_2 complexes into a bridging MNNM complex and a free N_2 molecule ($2\Delta G^{\circ}_{eq}$) is examined through systematic variations of the metal and ligands; values of ΔG°_{eq} range between +9.1 and -24.0 kcal/mol per M-N_2 bond. We propose a model that accounts for these broad variations by assigning a fixed π-bond order (BO^{π}) to the triatomic terminal MNN moiety that is equal to that of the free N_2 molecule, and a variable BO^{π} to the bridging complexes based on the character (bonding or antibonding) and occupancy of the π-MOs in the tetratomic MNNM core. When the conversion from terminal to bridging coordination and free N_2 is associated with an increase in the number of π-bonds ($\Delta BO^{\pi}_{eq} > 0$), the bridging mode is greatly favored; this condition is satisfied when each metal provides 1, 2 or 3 electrons to the π-MOs of the MNNM core. When each metal in the bridging complex provides 4 electrons to the MNNM π-MOs, $\Delta BO^{\pi}_{eq} = 0$; the equilibrium in this case is approximately ergoneutral and the direction can be shifted by dispersion interactions.

Introduction

Since their discovery in the mid-1960s,[1] transition metal dinitrogen complexes have been the subject of intense research as actual or model intermediates for catalytic transformations of N_2.[2] In particular, there is immense interest at present in developing molecular catalysts for the reduction of N_2 to ammonia which could provide a greener and more sustainable alternative to the century-old Haber-Bosch process.[3,4,5,6] With such catalysts, the reaction routes always begin with binding of N_2 to a metal center.

Dinitrogen complexes exhibit a variety of binding modes, and the two most common are terminal end-on (η^1-N_2) and bridging end-on (μ-η^1:η^1-N_2) as shown in Scheme 1.[7,8,9,10] For convenience, μ-N_2 is used throughout the manuscript to denote μ-η^1:η^1-N_2 end-on bridging coordination.[11]

Scheme 1. End-on N_2 coordination

M−N≡N	M-N≡N-M
η^1-N_2	μ-η^1:η^1-N_2

These two modes offer drastically different reaction pathways for subsequent reactivity.[12,13,14] For example, terminal N_2 ligands can undergo protonation at the terminal N atom, whereas this reaction is not observed in bridging analogues.[15] In the context of ammonia production using molecular catalysts, the protonation of a terminal MNN complex to give an MNNH intermediate is the beginning of the "Chatt cycle", which is a series of reductions and protonations at the distal nitrogen leading to ammonia and a terminal metal nitride (M≡N), as shown in Scheme 2.[16] Such a mechanism was likewise proposed for the first molecular catalyst capable of effecting N_2 reduction to NH_3.[17] This Chatt cycle route to ammonia is inhibited by formation of a bridging N_2 complex, and so a key design feature has been to avoid bridging N_2.

Scheme 2. Examples of alternative pathways for N_2 fixation

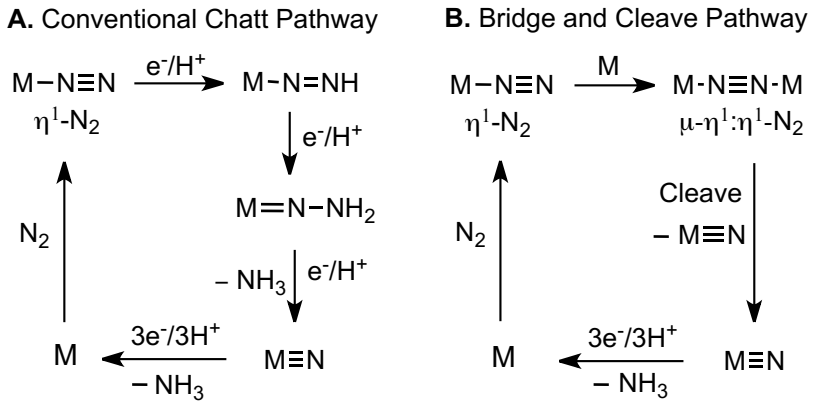

On the other hand, there is growing interest in designing complexes that can access a reduction mechanism featuring bridging MNNM followed by direct NN cleavage to form two terminal metal

nitride complexes (Scheme 2).[18,19] Such a cleavage pathway has been recently proposed for molecular catalysts that produce ammonia from N_2 using water as the proton source.[20] Obviously, the cleavage pathway requires a bridging N_2 intermediate to be formed from the initial terminal N_2 complex, essentially the opposite of the requirements for the Chatt cycle.

The direction and magnitude of the equilibrium between terminal and bridging end-on complexes (eq 1) is thus crucial for determining which pathways are available in a particular molecular system, which in turn dominates the principles used for catalyst design. This equilibrium may also be important in mechanisms of ammonia oxidation,[21] a subject of current interest in the context of carbon-free fuel cells.[22]

$$2\ MN_2 \underset{}{\overset{2\ \Delta G^{\circ}_{eq}}{\rightleftharpoons}} MNNM + N_2 \quad (1)$$

Despite the importance of this equilibrium, the factors determining its direction and magnitude have not been addressed in the literature.[23] To date, there exist no systematic quantitative data on ΔG°_{eq}, and no qualitative models for predicting whether terminal or bridging end-on N_2 will be favored as a function of metal identity, oxidation state, or ancillary ligands.

In this manuscript we present a new, intuitive method for determining whether electronic effects will lead N_2 to be terminal or end-on bridging in a given system based on the formal π-bond order in the MNNM core of the bridging complex. This model is built on experimental observations, and is supported through computations using density functional theory, which help to evaluate the various factors that influence the equilibrium (steric, dispersion, distortion, etc.). The model accounts for a surprisingly broad range of ΔG°_{eq} values computed for eq 1, ranging from +9.1 to –24.0 kcal/mol per M-N_2 bond. We describe first how this computational data lead to a π-bond order model by starting with octahedral d^5 and d^6 complexes of which examples of N_2 complexes with both bonding modes abound, then expanding to other metals, oxidation states, and geometries. Finally, we discuss the strengths and limitations of the new model.

Results and Discussion

Energy Decomposition Cycles. The thermodynamics of eq 1 were calculated for various complexes using the M06-L density functional[24] in a polarizable continuum representing toluene as solvent as described in the computational details section. The energy of eq 1 can have components from outer-sphere interactions between the ligands that are specific to the bridging complexes. These interactions can be attractive or repulsive, and can vary among the different classes of complexes. To be able to compare the intrinsic electronic energies of N_2 binding to M independently of the outer-sphere ligand-based interactions, we utilize the two thermodynamic cycles outlined in Scheme 3, which enable us to isolate the electronic effects that may drive a system to favor terminal or bridging binding.

Scheme 3. Thermodynamic cycles for terminal and bridged N_2 coordination to a metal fragment [(a)]

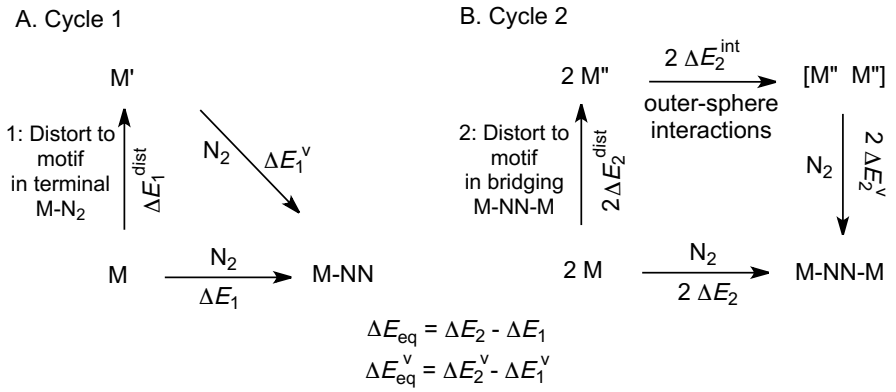

[(a)] M is the optimized metal fragment to which N_2 is being coordinated. M' or M" is the metal fragment after it has been distorted to its geometry in the terminal or bridged N_2 complex, respectively.

Both cycles start with free N_2 and unsaturated metal fragments, M. In the first cycle, the electronic energy ΔE_1 for terminal N_2 coordination to M is broken into: (i) $\Delta E_1^{\mathrm{dist}}$, the energy needed to distort M to the geometry M' it attains in the N_2 complex, and (ii) ΔE_1^{v}, the "vertical" (or adiabatic) binding energy of N_2 to M' without further geometry changes in the metal fragment. The second cycle breaks the electronic energy, 2 ΔE_2, of making the bridging complex MNNM from N_2 and two metal fragments into three terms: (i) $\Delta E_2^{\mathrm{dist}}$, the energy needed to distort each fragment M to its geometry M" in the bridged N_2 complex; (ii) 2 $\Delta E_2^{\mathrm{int}}$, the energy of the outer-sphere interactions due to combining the two distorted fragments into one [M" M"] adduct matching their positions and spin state in the bridging complex; and (iii) 2 ΔE_2^{v}, the "vertical" energy for bridged binding of N_2 to the [M" M"] adduct. For the purpose of understanding eq 1, the parameter of greatest interest in Scheme 3 is the difference $\Delta E_{\mathrm{eq}}^{\mathrm{v}} = \Delta E_2^{\mathrm{v}} - \Delta E_1^{\mathrm{v}}$, rather than the individual energies. $\Delta E_{\mathrm{eq}}^{\mathrm{v}}$ reflects purely electronic control over the terminal versus bridging coordination mode. Negative $\Delta E_{\mathrm{eq}}^{\mathrm{v}}$ values in eq 1 implicate electronic conditions that favor bridged coordination. Comparisons between $\Delta E_{\mathrm{eq}}^{\mathrm{v}}$ and $\Delta G_{\mathrm{eq}}^{\circ}$ can elucidate situations where outer-sphere effects or entropy and thermal terms may override electronic effects. To facilitate comparisons, all of the energy terms are normalized to one M-N_2 bond.

Scheme 4. Fragments investigated for terminal versus bridging N_2 binding in octahedral d^5 and d^6 complexes in Tables 1 and 2 [a,b]

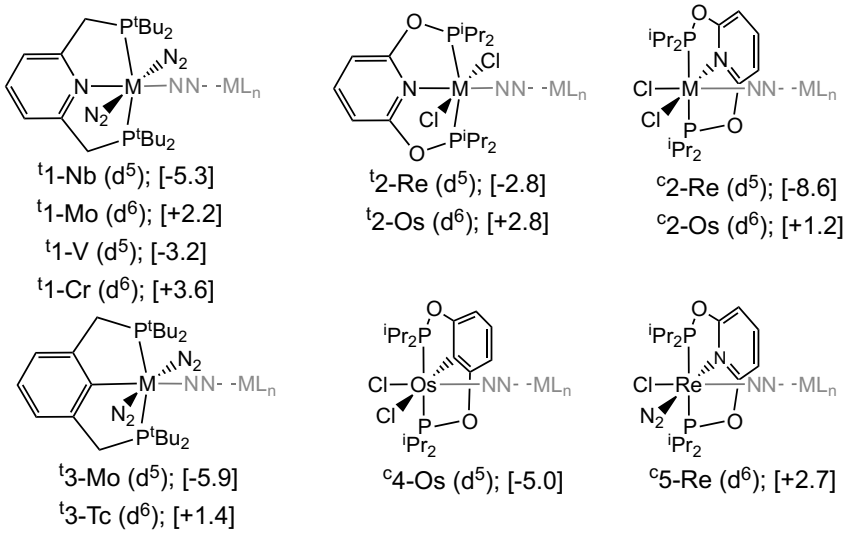

[a] For the ^{iPr}PONOP-M(Cl)$_2$ complexes the *trans,trans* and *cis,cis* isomers of the bridged N_2 complex were both considered. [b] Numbers in brackets are the ΔE^{v}_{eq} values defined in Scheme 3 in kcal/mol.

Table 1. Terminal vs. bridging N_2 binding in octahedral d^5 and d^6 complexes [a]

	Cycle 1 (terminal)		Cycle 2 (bridging)			Eq 1		
	ΔE_1^{dist}	ΔE_1^{v}	ΔE_2^{dist}	ΔE_2^{int}	ΔE_2^{v}	ΔE^{v}_{eq}	ΔE_{eq}	ΔG°_{eq}
^{t}**1**-Nb d^5	1.9 [b]	-30.9	3.3 [b]	-5.6	-36.2	-5.3	-9.5	-9.3
^{t}**1**-Mo d^6	0.9 [b]	-37.7	1.4 [b]	-5.4	-35.4	+2.2	-2.6	-2.9
^{Me}**1**-Mo d^6	1.2 [b]	-35.7	1.0 [b]	-1.0	-33.0	+2.8	+1.5	+1.3
^{t}**1**-V d^5	0.8 [b]	-30.1	2.1 [b]	-7.2	-33.4	-3.2	-9.1	-6.4
^{t}**1**-Cr d^6	0.9 [b]	-38.3	1.3 [b]	-6.2	-34.7	+3.6	-2.2	-0.9
^{t}**2**-Re d^5	7.8	-33.2	7.8	-4.3	-35.9	-2.8	-7.0	-5.0
^{t}**2**-Os d^6	7.8	-42.9	7.7	-5.4	-38.4	+4.5	-1.0	+0.8
^{c}**2**-Re d^5	8.7	-32.3	12.8	-7.2	-42.3	-10.0	-13.1	-9.8
^{c}**2**-Os d^6	10.9	-43.4	12.3	-8.5	-40.8	+2.6	-4.6	-0.7
^{t}**3**-Mo d^5	1.0	-22.4	2.1	-5.1	-28.3	-5.9	-9.9	-10.2
^{t}**3**-Tc d^6	1.2	-27.9	1.4	-5.1	-26.5	+1.4	-3.5	-1.3
^{c}**4**-Os d^5	19.1	-31.6	23.3	-7.7	-36.6	-5.0	-8.5	-5.3
^{c}**5**-Re d^6	10.8	-44.9	11.4	-7.0	-42.2	+2.7	-3.7	-1.6

[a] M06-L results in kcal/mol. The ΔE terms are defined in Scheme 3. [b] Distortion energies are given relative to the *trans* isomer of the [$(N_2)_2$(^{tBu}PNP)M] fragment.

Octahedral d^5 and d^6 Pincer Complexes. We exemplify the approach and some of the details of analyzing eq 1 with octahedral complexes derived from the five-coordinate fragments given in

Scheme 4, beginning with the complexes of the molybdenum(0) (bis)dinitrogen fragment *trans*-[(^{tBu}PNP)Mo(N_2)$_2$], ^{t}**1**-Mo.

Scheme 5. Experimentally observed bridging N_2 complexes derived from the 1-Mo and 2-Re fragments

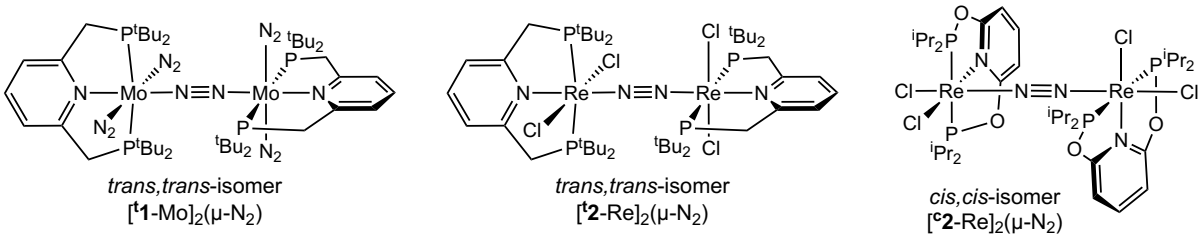

Nishibayashi and coworkers discovered a class of pincer-ligated N_2 complexes, typified by ^{t}**1**-Mo, that catalyze N_2 reduction to ammonia.[25] The catalytic precursor in this system was the *trans,trans* isomer of the N_2-bridging dimolybdenum complex shown in Scheme 5, and Raman and ^{15}N NMR spectroscopy indicated that the bridging mode is maintained when the solid is dissolved in THF under 1 atm N_2. In agreement with this observation, the computed ΔG°_{eq} (eq 1) for ^{t}**1**-Mo is -2.9 kcal/mol, indicating that bridging coordination is slightly favored over terminal coordination under 1 atm N_2. However, ΔE^{v}_{eq} in this system is +2.2 kcal/mol. This means that although eq 1 lies in the direction of μ-N_2, the terminal complex has a Mo-N_2 bond that is intrinsically stronger than the bridging bonds. The distortion energies ΔE_1^{dist} and ΔE_2^{dist} are low and comparable in this system, 0.9 and 1.4 kcal/mol, respectively, so their contributions to ΔG°_{eq} nearly cancel out. According to Scheme 3, therefore, the favorable formation of the N_2-bridged species [^{t}**1**-Mo]$_2$(μ-N_2) in eq 1 is driven by the outer-sphere interaction energy, ΔE_2^{dist} = -5.4 kcal/mol, which is sufficiently negative to offset ΔE^{v}_{eq}. The M06-L functional was designed to treat non-covalent interactions,[24,26] so the negative value of ΔE_2^{int} can be attributed to weak dispersion forces between the ligands of the two fragments in the bridged complex. On the other hand, density functionals that do not account for dispersion interactions afford *positive* values of ΔE_2^{int} and endergonic ΔG°_{eq}. For example, the B3LYP functional[27] gives ΔE_2^{int} = +1.8 and ΔG°_{eq} = +5.6 kcal/mol. Adding dispersion terms explicitly to the B3LYP energies through the empirical method of Grimme (D3BJ)[28,29] recovers the negative values of ΔE_2^{int} and ΔG°_{eq}: -7.4 and -3.5 kcal/mol, respectively.

The role of outer-sphere interactions in displacing the equilibrium of eq 1 for ^{t}**1**-Mo toward the bridged species can also be illustrated by substituting the *tert*-butyl groups of ^{t}**1**-Mo with methyl groups. Entry ^{Me}**1**-Mo in Table 1 shows that methyl/*tert*-butyl substitution has little effect on ΔE^{v}_{eq} (2.2 vs 2.8 kcal/mol), thus supporting the conclusion that the terminal Mo-N_2 bond is intrinsically stronger than each bridging bond. The substitution, however, reduces ΔE_2^{int} from -5.4 to -1.0 kcal/mol, thereby leaving ΔE^{v}_{eq} to drive eq 1 slightly in the direction of terminal M-N_2: ΔG°_{eq} = +1.3

kcal/mol. The spatial dimensions of the MNNM moiety for M = ^{t}**1**-Mo probably offer a balance of optimal dispersion interactions among the *tert*-butyl groups. This analysis suggests that relatively minor changes to the phosphine substituents could lead to significant changes in catalyst speciation during N_2 fixation catalysis. It is interesting that the same bulky alkyl substituents that are often introduced on the ligands to prevent dimerization by MM bond formation or through a single-atom bridge, in the N_2 case, instead, favor the bridged N_2 coordination. The importance of London dispersion forces in the reactions of organometallic compounds has been the subject of a recent review.[30]

Dinitrogen complexes of the d^5 rhenium(II) fragment, **2**-Re, were investigated by Bruch *et al*.[31] A related d^5-Re system with a different pincer PNP ligand was studied by the Schneider group.[32] Both systems are isolated as bridging N_2 complexes. In solution, these complexes undergo NN photocleavage into terminal metal-nitride species. For **2**-Re studied here the *trans,trans* isomer of the bridging complex [(^{iPr}PONOP)$ReCl_2$]$_2$(μ-N_2) was isolated initially. However, upon heating, this isomer converts in solution into the *cis,cis* isomer [^{c}**2**-Re]$_2$(μ-N_2) that features the pyridyl rings of the two pincer ligands in parallel planes as shown in Scheme 5. There was no evidence for a terminal N_2 complex under an N_2 atmosphere in this system, indicating that the equilibrium for eq 1 lies to the right.

In agreement with experimental observations, the computed ΔG°_{eq} for conversion of the *trans*-terminal N_2 adduct of ^{t}**2**-Re to the *trans,trans*-bridging isomer is negative, -5.0 kcal/mol (entry ^{t}**2**-Re in Table 1). In contrast to ^{t}**1**-Mo, ΔE^{v}_{eq} for the N_2 complexes of ^{t}**2**-Re and ^{c}**2**-Re are both negative, -2.8 and -10.0 kcal/mol, respectively, indicating the bridging MN bonds in this system are intrinsically stronger than the terminal bonds.

To more systematically explore changes in the thermodynamics of eq 1, several derivatives of **1**-Mo and **2**-Re that preserve overall charge neutrality were examined (Scheme 4). First, we introduced variations on ^{t}**1**-Mo. Fragments ^{t}**1**-Nb, ^{t}**1**-Cr and ^{t}**1**-V all retain the same ligands as ^{t}**1**-Mo, but with the Nb(0), Cr(0) and V(0) congeners. Fragment ^{t}**3**-Mo is an analogue of ^{t}**1**-Mo but with the anionic ^{tBu}PCP pincer ligand and molybdenum in the +I oxidation state. Finally, ^{t}**3**-Tc, is the technetium(I) analogue of ^{t}**3**-Mo. ^{t}**1**-Nb, ^{t}**1**-V and ^{t}**3**-Mo are all d^5-metal fragments, and their N_2 products in eq 1 give ΔE^{v}_{eq} = -5.3, -3.2 and -5.9 kcal/mol, respectively. ^{t}**1**-Cr and ^{t}**3**-Tc, on the other hand, are d^6 complexes that give positive ΔE^{v}_{eq} values in eq 1: +3.6 and +1.4 kcal/mol, respectively.

Next, we varied **2**-Re. The N_2 complexes of the d^6 (^{iPr}PONOP)$Os(Cl)_2$ fragments ^{t}**2**-Os and ^{c}**2**-Os both give positive ΔE^{v}_{eq}: +4.5 and +2.6 kcal/mol, respectively. In contrast, the complexes from the d^5 Os^{III} ^{iPr}POCOP analogue of **2**-Re, ^{c}**4**-Os in Scheme 4, give ΔE^{v}_{eq} = -5. kcal/mol. Finally, the terminal and bridging N_2 products from the d^6 Re(I) fragment ^{c}**5**-Re with ^{iPr}PONOP, one chloride and one N_2 ligand give ΔE^{v}_{eq} = +2.7 kcal/mol.

The components of cycles 1 and 2 in Table 1 exhibit pronounced variations among the different complexes studied, including the individual ΔE_1^{v} and ΔE_2^{v} components. Nevertheless, $\Delta G_{\mathrm{eq}}^{\circ}$ is within 3 kcal/mol of ergoneutral in all the d^6 systems investigated, and significantly more exergonic for the d^5 systems, ranging from -5.3 to -10.2 kcal/mol. An even sharper division is found in the $\Delta E_{\mathrm{eq}}^{\mathrm{v}}$ data which are positive for all of the d^6-complexes and systematically negative for the d^5 ones, with averages of +2.8 and -5.4 kcal/mol, respectively. The general result for $\Delta E_{\mathrm{eq}}^{\mathrm{v}}$ is independent of the density functional, the basis set, solvation, and whether dispersion effects are accounted for or not.

A π-Bond Order Model. The $\Delta E_{\mathrm{eq}}^{\mathrm{v}}$ data in Table 1 implicate an electronic effect that favors bridging N_2 coordination in the octahedral d^5 complexes but not in the d^6 ones. To elucidate the origin of this effect, we inspect in Fig. 1 the π-MOs in the octahedral terminal and bridging N_2 complexes of the symmetrical d^6 fragment $[HRe(NH_3)_4]$. The ammonia and hydride ligands in $[HRe(NH_3)_4]$ prevent π-MO delocalization beyond the M-N_2 core of interest, which was observed for the complexes in Scheme 4 (Fig S1-S4) and which is known to plague MO analyses of other studies of related complexes.[32,33] To aid the discussion we also utilize general qualitative π-MO diagrams for free N_2 and the MNN and MNNM moieties.

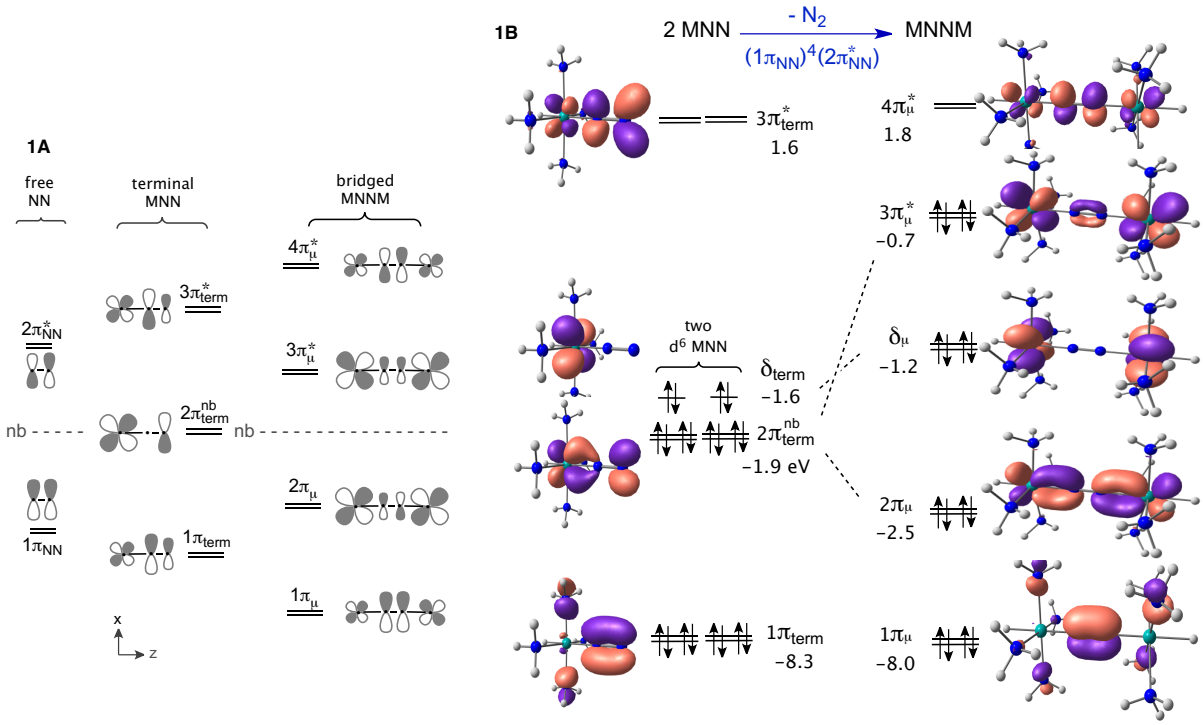

Figure 1. Schematic π-MOs in NN, MNN and MNNM, and Kohn-Sham MOs of the terminal and bridging N_2 complexes of the fragment d^6-[$HRe(NH_3)_4$]; MO energies in eV.

Part A of Fig. 1 shows the two pairs of π-MOs (each doubly degenerate) of the free N_2 molecule: one bonding and one antibonding, $1\pi_{NN}$ and $2\pi^*_{NN}$, respectively. The filling of four electrons in $1\pi_{NN}$ leads to a π-bond order of 2 ($BO^{\pi}_{NN} = 2$). A terminal end-on MNN complex introduces two metal d-orbitals with appropriate symmetry for π-bonding with N_2 leading to a total of three pairs of π-symmetry MOs. For a simplified situation in which the AOs are similar in energy, as in the allyl group for example,[34] the three pairs of π-MOs in the terminal MNN motif have the following characters: $1\pi_{term}$ is the all in-phase bonding MO, $2\pi^{nb}_{term}$ is non-bonding with a node at the central atom, and $3\pi^*_{term}$ is all out-of-phase antibonding.

Figure 1B displays the Kohn-Sham π-MOs computed for the ReNN moiety of the complex [$HRe(NH_3)_4(N_2)$], along with the metal based d_{xy} orbital of δ symmetry with respect to the MNN bond (δ_{term}). The π-MOs have the uneven atomic contributions expected based on the different electronegativities of nitrogen and rhenium. $1\pi_{term}$ is localized almost exclusively on the two N atoms of Re-NN. The second π-MO has major contributions from rhenium and the distal nitrogen, but only a minor component from the proximal nitrogen atom. This is reminiscent of the second π-MO in the allyl group, so by analogy we denote the MO in ReNN also as formally "non-bonding" ($2\pi^{nb}_{term}$). Finally, the all-antibonding $3\pi^*_{term}$ has large contributions from the two N atoms along with a small but significant contribution from the metal. The analogy between the valence π-MO in MNN and the allyl group was noted by DuBois and Hoffmann.[35]

The "allyl-like" view of π-bonding in MNN implies that the different population of $2\pi^{nb}_{term}$ in related d^5 and d^6 terminal N_2 complexes, $(2\pi^{nb}_{term})^3$ and $(2\pi^{nb}_{term})^4$ respectively, should have no major effects on the M-N (r_{MN}) and NN (r_{NN}) bond distances. This is strikingly different from the traditional backbonding model that is dominated by in-phase mixing between filled metal d-AOs and π^*_{NN}. The latter model would be expected to lead to significantly shorter r_{MN}, longer r_{NN} and lower NN stretch frequencies in the d^6 complexes, but this is not consistent with the computed data. As illustrated for selected examples in Table 2, the four pairs of terminal congeners with $(2\pi^{nb}_{term})^3$ vs $(2\pi^{nb}_{term})^4$ configurations (^{t}**1**-M, ^{c}**2**-M, ^{t}**2**-M and ^{t}**3**-M) are computed to have M-N bond distances, r_{MN}, that are significantly shorter (by 0.07 Å on average) for the d^6 complexes versus their d^5 congeners. However, the NN distances in these complexes, r_{NN}, are independent of the occupancy of $2\pi^{nb}_{term}$, in fact all four d^6 complexes have *shorter* r_{NN}, (albeit negligibly, 0.001 to 0.004 Å; Δr_{NN} in Table 2) and significantly *higher* NN vibrational stretch frequency ν_{NN} (by 43 to 55 cm^{-1}) than their d^5-counterparts. Clearly, the computed trends in r_{MN}, r_{NN} and ν_{NN} cannot be all explained by either qualitative π-model alone. However, an important feature of triatomic molecules that becomes highlighted in the allyl-like analogy is that a terminal MNN moiety should have a total $BO^{\pi}_{term} = 2$ resulting, formally, from the lowest filled $1\pi_{term}$ MO regardless of the occupancy of $2\pi^{nb}_{term}$. Since $1\pi_{term}$ is concentrated largely on NN, the given BO^{π}_{term} can be expressed using the M-N≡N Lewis structure, which captures the relatively short NN bond length computed for all of the terminal complexes.

Table 2. M-N and N-N bond lengths (in Å) and N-N stretching vibration frequencies (in cm^{-1}) for selected octahedral complexes from Table 1 [a]

	Terminal M-N_2			Bridging MNNM				Eq 1		
Frag.	r_{MN}	r_{NN}	ν_{NN}	d^n_π-d^n_π	r_{MN}	r_{NN}	ν_{NN}	Δr_{MN}	Δr_{NN}	ΔBO^{π}_{eq}
^{t}**1**-Nb d^5	2.113	1.135	2026	d^3_π-d^3_π	1.973	1.189	1678	-0.140	0.054	**1**
^{t}**1**-Mo d^6	2.018	1.134	2070	d^4_π-d^4_π	2.012	1.153	1976	-0.006	0.019	**0**
^{t}**2**-Re d^5	1.975	1.128	2129	d^3_π-d^3_π	1.923	1.155	1940	-0.052	0.027	**1**
^{t}**2**-Os d^6	1.935	1.124	2184	d^4_π-d^4_π	1.944	1.134	2173	0.009	0.010	**0**
^{c}**2**-Re d^5	1.978	1.131	2095	d^3_π-d^3_π	1.909	1.175	1843	-0.069	0.044	**1**
^{c}**2**-Os d^6	1.912	1.130	2142	d^4_π-d^4_π	1.950	1.144	2101	0.038	0.014	**0**
^{t}**3**-Mo d^5	2.119	1.127	2094	d^3_π-d^3_π	1.993	1.169	1831	-0.126	0.042	**1**
^{t}**3**-Tc d^6	2.041	1.126	2137	d^4_π-d^4_π	2.053	1.140	2067	0.012	0.014	**0**

[a] Complexes described in Scheme 4. d^n_π-d^n_π specifies the number of d electrons provided by each metal to the π-MOs of MNNM. ΔBO^{π}_{eq} is defined in eq 2.

A different situation applies in the bridging complexes. In the tetratomic MNNM core, eight π-AOs transform into four doubly degenerate π_μ-MOs: two with bonding ($1\pi_\mu$ and $2\pi_\mu$) and two with

antibonding character ($3\pi_\mu^*$ and $4\pi_\mu^*$) as described schematically in Fig. 1A. The Kohn-Sham MOs of $[HRe(NH_3)_4]_2(\mu\text{-}N_2)$ show $1\pi_\mu$ to be localized on the two bridging nitrogen atoms, similar to $1\pi_{term}$ in $[HRe(NH_3)_4(N_2)]$. In stark contrast to $2\pi_{term}^{nb}$ in the terminal-N_2 complex, $2\pi_\mu$ in the bridged complex has large in-phase overlap between the metal and nitrogen AOs of the MN bonds. Consistent with the implied bonding character of this MO, the energy of $2\pi_\mu$ is 1.3 eV below the two, formally non-degenerate, non-bonding δ_μ MOs from the two linear combinations of the d_{xy} AOs of the two metals. The display of $3\pi_\mu^*$ in $[HRe(NH_3)_4]_2(\mu\text{-}N_2)$, on the other hand, shows it to be highly localized on the metals with minor contributions from the nitrogen AOs. Nevertheless, the energy of $3\pi_\mu^*$ is 0.5 eV above δ_μ reflecting an acquired antibonding character as would be expected from the phasing of four atomic orbitals which requires a net of two π-nodes in this MO, one in each of the M-N bonds. Finally, $4\pi_\mu^*$ is all π-antibonding but with greater atomic coefficients from the N atoms than from the metal d-AOs. Since there are no non-bonding π-MOs in the tetratomic MNNM core, the formal π-bond order in the bridging complexes (BO_μ^π) should depend on the total number of electrons in π-symmetry d-orbitals supplied by the two metals (d_π^n-d_π^n in Table 2). Note that d_π^n is distinct from the total d-electron count d^n. In the d^6-d^6 systems, each metal provides four electrons to the π-MOs of MNNM (d_π^4-d_π^4), so the full π-electron configuration is $(1\pi_\mu)^4(2\pi_\mu)^4(3\pi_\mu^*)^4(4\pi_\mu^*)^0$. In this case, the equal occupancy of $2\pi_\mu$ bonding and $3\pi_\mu^*$ antibonding orbitals leads to MNNM with $BO_\mu^\pi = 2$ (arising from the pair of filled $1\pi_\mu$ bonding MOs). Since $1\pi_\mu$ is concentrated on NN, the dominant Lewis structure in a d^6-d^6 μ-N_2 complex would be M-N≡N-M, with the two π-bonds localized between the two nitrogen atoms, similar to the case in the terminal M-N≡N. In the d^5-d^5 systems, on the other hand, each metal provides only three electrons to MNNM (d_π^3-d_π^3), so $2\pi_\mu$ remains completely filled while the antibonding $3\pi_\mu^*$ is only partially filled; hence BO_μ^π increases to 3. Based on the position of the nodes, this depletion of $3\pi_\mu^*$ would increase the bonding character of the MN bond and decrease that of the NN bond compared to a d_π^4-d_π^4 MNNM core, so an adequate Lewis structure for the d_π^3-d_π^3 MNNM core, with $BO_\mu^\pi = 3$, would be M=N=N=M. Consistent with this analysis, the d^5-d^5 complexes in Table 2 systematically have r_{MN} distances 0.02 to 0.06 Å *shorter* and similarly r_{NN} distances longer than their d^6-d^6 congeners. In accord with the different NN bond distances, ν_{NN} is computed to be systematically much lower in the d^5-d^5 complexes than the d^6-d^6 ones (Table 2).

Considering eq 1 through the lens of Fig. 1, we define in eq 2 the term ΔBO_{eq}^π, the change in the π-bond order when converting two terminal complexes into a bridging complex and a free N_2 as shown.

$$\Delta BO_{eq}^\pi = BO_\mu^\pi + BO_{NN}^\pi - 2BO_{term}^\pi \quad (2)$$

According to the above discussion, $BO^{\pi}_{term} = 2$ regardless of the numbers of π-electrons provided by the metal. Since $BO^{\pi}_{NN} = 2$ as well, ΔBO^{π}_{eq} depends only on BO^{π}_{μ} (eq 3).

$$\Delta BO^{\pi}_{eq} = BO^{\pi}_{\mu} - 2 \qquad (3)$$

The variations in BO^{π}_{μ} brought by the occupancy of the π-MOs in the bridging complex, therefore, lead to variations in ΔBO^{π}_{eq} in eq 1 as outlined in Scheme 6.

Scheme 6. Relating the π-electron configuration of MNNM to ΔBO^{π}_{eq} and ΔE^{v}_{eq} of eq 1[(a)]

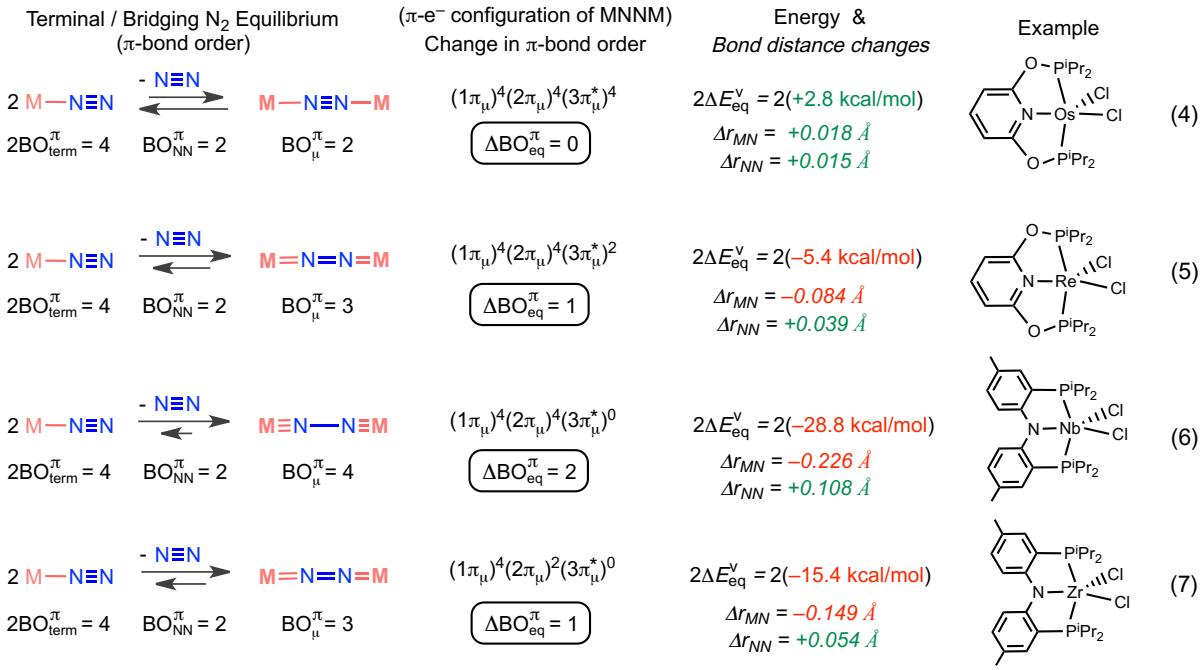

[(a)] ΔBO^{π}_{eq} is defined in eq 2. Δr_{MN} and Δr_{NN} are the differences in the MN and NN bond distances in the bridging and terminal N_2 complexes. Energy and bond distance values are the averages of the octahedral complexes in Tables 1-4.

In the reactions of d^6 complexes, the d^6-d^6 bridging complex has $(2\pi_{\mu})^4(3\pi^*_{\mu})^4$ configuration with $BO^{\pi}_{\mu} = 2$, the same as BO^{π}_{term}, so $\Delta BO^{\pi}_{eq} = 0$ (eq 4 in Scheme 6). In the d^5 systems, on the other hand, the d^5-d^5 bridging complex has $(2\pi_{\mu})^4(3\pi^*_{\mu})^2$ configuration with $BO^{\pi}_{\mu} = 3$. In this case MNN to MNNM conversion is a reaction that creates one additional π-bond in the bridging complex so $\Delta BO^{\pi}_{eq} = 1$ (eq 5 in Scheme 6). These different ΔBO^{π}_{eq} align perfectly with the computed trends in ΔE^{v}_{eq}, where the d^5-d^5 systems that introduce an additional bond in the bridged complex favor bridging N_2 coordination and the d^6-d^6 systems slightly favor terminal N_2 coordination.

The different ΔBO^{π}_{eq} indicated by the above MO-analysis for the d^5 and d^6 systems is well supported by the structural data and vibrational frequencies in Table 2. For the d^6-systems, the transformation from MNN to MNNM is associated with a minor increase in both the MN and NN bond distances: $\Delta r_{MN} = 0.018$ Å and $\Delta r_{NN} = 0.015$ Å, on average. In these reactions the average

change in ν_{NN} is only -61 cm^{-1}. In contrast, bridging in the d^5 systems causes significant *contraction* in r_{MN} and significant lengthening in r_{NN} compared to the terminal complexes: Δr_{MN} = -0.083 Å and Δr_{NN} = 0.039 Å, on average. Accordingly, the average change in ν_{NN} in the formation of the d^5-d^5 bridged complexes is substantial: -246 cm^{-1}.

We hypothesized that the π-BO approach for rationalizing the direction of eq 1 taken for octahedral d^5 and d^6 complexes would be applicable to metal N_2 complexes broadly. In the following sections we test this hypothesis by exploring other d_π^n-d_π^n configurations and coordination numbers.

Octahedral d^4 – d^1 Complexes. The above MO-based arguments imply that the MNNM core acquires a maximum of 4 π-bonds when the $2\pi_\mu$ MO is full and the $3\pi_\mu^*$ MO is empty. The matching Lewis structure for this configuration would be M≡N-N≡M, analogous to butadiyne. In this case eq 1 will have the maximal $\Delta BO_{eq}^{\pi} = 2$ (eq 6 in Scheme 6) and the equilibrium would be increasingly shifted to the right in favor of bridging coordination. This condition requires each metal to supply only two electrons to the π-MOs of MNNM (d_π^2-d_π^2), which can in principle be achieved in octahedral d^4, d^3 and d^2 metal systems, depending upon the occupancy of the non-bonding δ_μ MOs. We calculated examples in these categories, shown in Scheme 7. The results are given in Tables 3 and 4.

Scheme 7. Fragments investigated for terminal vs. bridging N_2 binding in octahedral d^4 – d^1 complexes (Tables 3 and 4)

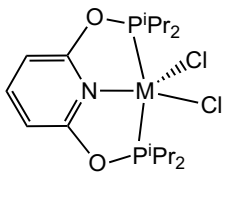

^{c}2-W (d^4); ^{c}2-Ta (d^3)

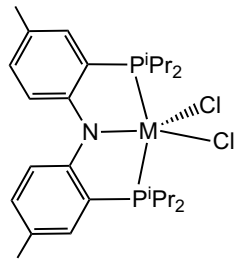

^{c}6-Nb (d^2); ^{c}6-Zr (d^1)

Table 3. Terminal vs. bridging N_2 binding in octahedral d^4 – d^1 complexes [(a)]

	Cycle 1 (terminal)		Cycle 2 (bridging MNNM)				Eq 1			
	ΔE_1^{dist}	ΔE_1^{v}	ΔE_2^{dist}	ΔE_2^{int}	ΔE_2^{v}	$(2\pi_\mu)^m(\delta_\mu)^n(3\pi_\mu^*)^0$	ΔE_{eq}^{v}	ΔE_{eq}	ΔG_{eq}°	$\mathbf{\Delta BO_{eq}^{\pi}}$
[c]2-W d^4	14.5	-38.3	27.1	-5.9	-64.2	$(2\pi_\mu)^4(\delta_\mu)^4(3\pi_\mu^*)^0$	-25.9	-19.2	-14.6	**2**
[c]2-Ta d^3	10.8	-31.1	19.0	-12.1	-56.6	$(2\pi_\mu)^4(\delta_\mu)^2(3\pi_\mu^*)^0$	-25.5	-29.4	-24.0	**2**
[c]6-Nb d^2	15.2	-20.0	33.6	-7.3	-55.0	$(2\pi_\mu)^4(\delta_\mu)^0(3\pi_\mu^*)^0$	-35.0	-23.9	-17.8	**2**
[c]6-Zr d^1	5.0	-17.0	9.0	-2.1	-32.5	$(2\pi_\mu)^2(\delta_\mu)^0(3\pi_\mu^*)^0$	-15.5	-13.6	-6.5	**1**

[(a)] Complexes described in Scheme 7. M06-L results in kcal/mol. The ΔE terms are defined in Scheme 3. ΔBO_{eq}^{π} is defined in eq 3. $(2\pi_\mu)^m(\delta_\mu)^n(3\pi_\mu^*)^0$ is the valence π-MO configuration in the bridging complex.

Table 4. M-N and N-N bond lengths (in Å) and N-N stretch vibration frequencies (in cm^{-1}) for octahedral d^4 – d^1 complexes [a]

	Terminal M-N_2			Bridging MNNM				Eq 1		
Frag.	r_{MN}	r_{NN}	ν_{NN}	d_π^n-d_π^n	r_{MN}	r_{NN}	ν_{NN}	Δr_{MN}	Δr_{NN}	$\mathbf{\Delta BO_{eq}^{\pi}}$
[c]2-W d^4	1.996	1.141	2017	d_π^2-d_π^2	1.831	1.239	1512	-0.165	0.098	**2**
[c]2-Ta d^3	2.086	1.141	1966	d_π^2-d_π^2	1.871	1.255	1457	-0.215	0.114	**2**
[c]6-Nb d^2	2.178	1.124	2120	d_π^2-d_π^2	1.879	1.237	1457	-0.299	0.113	**2**
[c]6-Zr d^1	2.322	1.122	2142	d_π^1-d_π^1	2.173	1.177	1786	-0.149	0.055	**1**

[a] Complexes described in Scheme 7. d_π^n specifies the number of d electrons provided by each metal to the π-MOs in MNNM. ΔBO_{eq}^{π} is defined in eq 2.

Table 3 begins with N_2 binding to **[c]2**-W, a d^4 analog of d^5 [c]**2**-Re. The [(^{iPr}PONOP)WCl_2] fragment and the octahedral [**[c]2**-W]-N_2 have triplet ground states. The *cis,cis*-bridging complex [**[c]2**-W]$_2$(μ-N_2), on the other hand, has a closed shell singlet ground state from the $(1\pi_\mu)^4(2\pi_\mu)^4(\delta_\mu)^4(3\pi_\mu^*)^0$ configuration.[36,37] The geometry of [**[c]2**-W]$_2$(μ-N_2) features two very short MN bonds and an elongated NN bond (1.83 and 1.24 Å, respectively, in Table 4) supporting the suitability of the M≡N-N≡M Lewis structure. Terminal N_2 binding to **[c]2**-W does not change the spin state, but requires a major change in the geometry of the fragment, so the distortion energy in the first thermodynamic cycle in Scheme 3 is relatively high: ΔE_1^{dist} = 14.5 kcal/mol (Table 3). On the other hand, making the closed shell [**[c]2**-W]$_2$(μ-N_2) in cycle 2 requires a major change in the geometry of the fragment as well as a change in the spin state, which leads to a very high ΔE_2^{dist} (27.1 kcal/mol). Factoring out the very different distortion energies affords ΔE_{eq}^{v} = -25.9 kcal/mol, fully consistent with the proposed introduction of two new π-bonds upon conversion from terminal to bridged N_2 binding in eq 1 (ΔBO_{eq}^{π} = 2). Naturally, since ΔE_2^{dist} is much higher than ΔE_1^{dist}, the net preference for μ-N_2 binding as determined by ΔG_{eq}° (-14.6 kcal/mol) is significantly less than ΔE_{eq}^{v}. Nonetheless, the given ΔG_{eq}° is more exergonic than for any of the d^5 systems in Table 1 (-5.0 to -10.2 kcal/mol).

Next considered in Table 3 is the d^3 **ᶜ2**-Ta congener of **ᶜ2**-W. The bridged [**ᶜ2**-Ta]$_2$(μ-N_2) has a $(2\pi_\mu)^4(\delta_\mu)^2(3\pi_\mu^*)^0$ d^3-d^3 configuration with a geometry consistent with the M≡N-N≡M Lewis structure (Table 4). Again, for this system, ΔE^{v}_{eq} and ΔG°_{eq} in eq 1 are highly negative, -25.5 and -24.0 kcal/mol, respectively. The nearly equal ΔE^{v}_{eq} for d^3 **ᶜ2**-Ta and d^4 **ᶜ2**-W reflects the fact that the difference in the number of d-electrons between these species is only manifested in the population of the non-bonding δ_μ-MOs and hence does not change ΔBO^{π}_{eq}.

The third condition for maximal ΔBO^{π}_{eq} for eq 1 is represented by d^2 fragments leading to μ-N_2 complexes with a $(2\pi_\mu)^4(\delta_\mu)^0(3\pi_\mu^*)^0$ configuration. Several μ-N_2 examples of this kind are experimentally known.[38,39] Scheme 6 considers the Nb(III) complex derived from the **ᶜ6**-Nb fragment with the diarylamido-diphosphine pincer ligand studied by the Mindiola group.[40] In accord with the proposed ΔBO^{π}_{eq} = 2, we compute this system to greatly favor bridging over terminal N_2 coordination: ΔE^{v}_{eq} = -35.0 and ΔG°_{eq} = -17.8 kcal/mol.

As a further demonstration of the direct relationship between the occupancy of the $2\pi_\mu$ and $3\pi_\mu^*$ MOs and the energy of eq 1, a system involving an MNNM core with a $(2\pi_\mu)^2(\delta_\mu)^0(3\pi_\mu^*)^0$ configuration is evaluated in Table 3 using **ᶜ6**-Zr which bears the same ligand of **ᶜ6**-Nb and the d^1-Zr^{III} metal center. The partial filling of the bonding $2\pi_\mu$ reduces the BO^{π}_{μ} in MNNM to 3, resulting in ΔBO^{π}_{eq} = 1 (eq 7 in Scheme 6). In this case bridging is still expected to be preferred over terminal coordination, but not as much as in **ᶜ6**-Nb. Indeed, ΔE^{v}_{eq} and ΔG°_{eq} for **ᶜ6**-Zr are -15.5 and -6.5 kcal/mol, respectively, as compared with -35.0 and -17.8 kcal/mol respectively for **ᶜ6**-Nb.

The structural parameters and vibrational frequencies of the N_2 complexes of **ᶜ6**-Zr and **ᶜ6**-Nb in Table 4 offer another illustration of the contrasting effects of varying the population of the $2\pi^{nb}_{term}$ and $2\pi_\mu$ MOs. Despite the different occupancies, $(2\pi^{nb}_{term})^1$ vs $(2\pi^{nb}_{term})^2$, the NN bond distance and ν_{NN} in the terminal [**ᶜ6**-Zr]-N_2 and [**ᶜ6**-Nb]-N_2 complexes are essentially the same: 1.122 vs 1.124 Å, and 2142 vs 2120 cm^{-1}, highlighting the lack of N-N antibonding character in $2\pi^{nb}_{term}$. In contrast, the N-N bond is significantly longer in N_2-bridged **ᶜ6**-Zr than in the terminal complex, and it is 0.060 Å longer still in N_2-bridged **ᶜ6**-Nb. The bridged complexes in this case have very different ν_{NN}: 1786 cm^{-1} versus 1457 cm^{-1}. Furthermore, the change from terminal to bridged coordination results in contraction of the M-N distance in **ᶜ6**-Nb by twice as much as in **ᶜ6**-Zr (-0.299 Å and -0.149 Å respectively), underscoring the much greater M-N bonding character of $2\pi_\mu$ compared with $2\pi^{nb}_{term}$.

Non-Octahedral Geometries. In this section we evaluate if the ΔBO^{π}_{eq} term as applied in Scheme 5 for octahedral complexes can also account for the computed energies of eq 1 in non-octahedral systems. For this purpose we consider a set of experimentally known five-, four- and three-coordinate N_2 complexes derived from the fragments given in Scheme 8. The results are collected in Tables 5

and 6. Note that in each case where ΔBO_{eq}^{π} is zero, the formation of a bridging N_2 complex is slightly unfavorable (with one minor exception, fragment **8**-Fe, with ΔG_{eq}° = -0.9 kcal/mol although ΔE_{eq} is positive, 0.7 kcal/mol), while in each case where ΔBO_{eq}^{π} is greater than zero, bridge formation is favorable.

Scheme 8. Fragments investigated for terminal versus bridging N_2 binding in the non-octahedral complexes evaluated in Tables 5 and 6

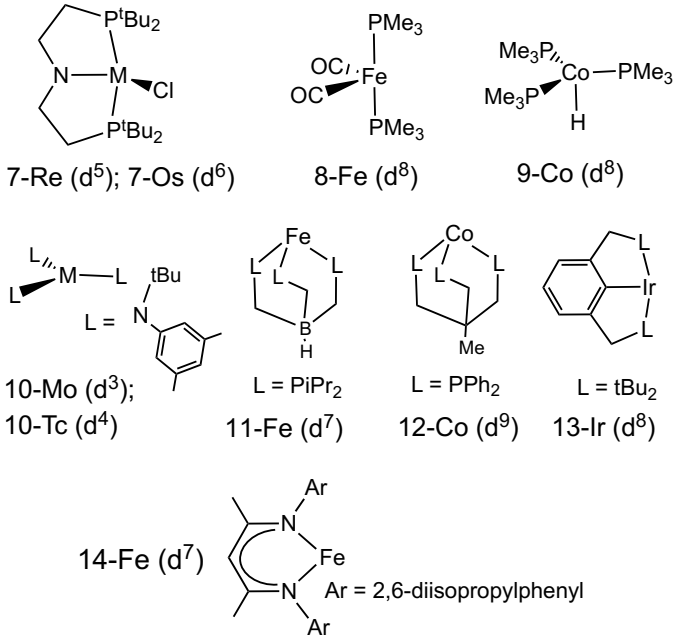

Table 5. Terminal versus bridging N_2 binding in five, four and three coordinate complexes [a]

	Cycle 1 (terminal)		Cycle 2 (bridging MNNM)				Eq 1			
	$\Delta E_1^{\mathrm{dist}}$	ΔE_1^{v}	$\Delta E_2^{\mathrm{dist}}$	$\Delta E_2^{\mathrm{int}}$	ΔE_2^{v}	$(2\pi_\mu)^m(3\pi_\mu^*)^n$	$\Delta E_{\mathrm{eq}}^{\mathrm{v}}$	ΔE_{eq}	$\Delta G_{\mathrm{eq}}^{\circ}$	$\mathbf{\Delta BO_{eq}^{\pi}}$
	Five-coordinate N_2 complexes									
7-Re d^5	5.2	-25.5	9.1	-2.7	-36.2	$(2\pi_\mu)^4(3\pi_\mu^*)^2$	-10.8	-9.5	-6.9	**1**
7-Os d^6	12.3	-33.2	14.2	-7.3	-26.6	$(2\pi_\mu)^4(3\pi_\mu^*)^4$	+6.5	+1.2	+3.6	**0**
8-Fe d^8	4.1	-32.2	4.2	-2.6	-29.0	$(2\pi_\mu)^4(3\pi_\mu^*)^4$	+3.2	+0.7	-0.9	**0**
9-Co d^8	16.5	-39.9	18.1	-4.6	-35.0	$(2\pi_\mu)^4(3\pi_\mu^*)^4$	+4.9	+1.9	+3.2	**0**
9-Fe d^7	16.7	-44.1	16.0	-4.9 [b]	-35.0	$(2\pi_\mu)^4(3\pi_\mu^*)^4$	+8.7	+3.1	+3.9	**0**
	Four-coordinate N_2 complexes									
10-Mo d^3	20.7 [c]	-28.2	20.8 [c]	-4.7	-40.6	$(2\pi_\mu)^4(3\pi_\mu^*)^2$	-12.4	-17.0	-11.6	**1**
10-Tc d^4	7.7	-42.6	9.3	-1.3	-38.8	$(2\pi_\mu)^4(3\pi_\mu^*)^4$	+3.8	+4.1	+9.1	**0**
11-Fe d^7	2.6	-26.8	3.8	-4.1	-28.4	$(2\pi_\mu)^4(3\pi_\mu^*)^2$	-1.6	-4.8	-3.9	**1**
12-Co d^9	4.1	-37.6	7.7	-9.6	-38.9	$(2\pi_\mu)^4(3\pi_\mu^*)^2$	-1.4	-7.4	-5.0	**1**
13-Ir d^8	2.2	-31.8	3.1	-3.4	-29.4	$(2\pi_\mu)^4(3\pi_\mu^*)^4$	+2.4	-0.1	+1.6	**0**
	Three-coordinate N_2 complexes									
14-Fe d^7	4.3	-34.7	3.3	-8.8 [b]	-38.1	$(2\pi_\mu)^4(3\pi_\mu^*)^2$	-3.3	-13.1	-9.3	**1**

[a] Complexes described in Scheme 8. M06-L results in kcal/mol. The ΔE terms are defined in Scheme 3. ΔBO_{eq}^{π} is defined in eq 2. $(2\pi_\mu)^m(3\pi_\mu^*)^n$ pertains to the N_2-bridged product. [b] $\Delta E_2^{\mathrm{int}}$ is evaluated using the B3LYP-D3J functional. [c] $\Delta E_1^{\mathrm{dist}}$ and $\Delta E_2^{\mathrm{dist}}$ account for a change in the spin state from quartet to doublet.

Table 6. M-N and N-N bond lengths (in Å) and N-N stretch vibration frequencies (in cm^{-1}) for non-octahedral complexes [a]

	Terminal M-N_2			Bridging MNNM				Eq 1		
Frag.	r_{MN}	r_{NN}	ν_{NN}	d_π^n-d_π^n	r_{MN}	r_{NN}	ν_{NN}	Δr_{MN}	Δr_{NN}	ΔBO_{eq}^{π}
Five coordinate N_2 complexes										
7-Re d^5	1.941	1.140	2016	d_π^3-d_π^3	1.885	1.186	1772	-0.056	0.046	**1**
7-Os d^6	1.900	1.135	2100	d_π^4-d_π^4	1.940	1.153	2038	+0.040	0.018	**0**
8-Fe d^8	1.783	1.130	2150	d_π^4-d_π^4	1.808	1.143	2104	+0.025	0.013	**0**
9-Co d^8	1.796	1.136	2104	d_π^4-d_π^4	1.827	1.154	2014	+0.031	0.018	**0**
9-Fe d^7	1.846	1.128	2162	d_π^4-d_π^4	1.860	1.143	2086	+0.014	0.015	**0**
Four coordinate N_2 complexes										
10-Mo d^3	1.916	1.147	1962	d_π^3-d_π^3	1.861	1.203	1726	-0.055	0.056	**1**
10-Tc d^4	1.849	1.144	2044	d_π^4-d_π^4	1.913	1.161	1977	+0.064	0.017	**0**
11-Fe d^7	1.811	1.133	2115	d_π^3-d_π^3	1.761	1.175	1876	-0.050	0.042	**1**
12-Co d^9	1.871	1.130	2124	d_π^3-d_π^3	1.810	1.169	1874	-0.061	0.039	**1**
13-Ir d^8	1.958	1.129	2144	d_π^4-d_π^4	2.022	1.145	2039	+0.064	0.016	**0**
Three coordinate N_2 complexes										
14-Fe d^7	1.823	1.136	2105	d_π^3-d_π^3	1.782	1.174	1919	-0.040	0.040	**1**

[a] Complexes described in Scheme 8. d_π^n is the number of electrons provided by each metal to the π-MOs of MNNM.

The Schneider group has prepared the five-coordinate bridging d^5-d^5 complex [(^{tBu}PNP)ReCl]$_2$(μ-N_2) (**7**-Re in Scheme 8) which undergoes a facile cleavage of the bridging N_2 ligand at room temperature.[41,42] No terminal N_2 complex was detected in this system. In contrast, terminal N_2 bonding has been observed in five coordinate d^6-Tc^I and d^6-Os^{II} PNP pincer complexes.[43,44] [**7**-Re]$_2$(μ-N_2) has two unpaired electrons in $3\pi_\mu^*$; therefore, for eq 1, $\Delta BO_{eq}^{\pi} = 1$, and according to the above discussion the bridging M-N_2 bonds are expected to be stronger than the terminal M-N_2 ones. Consistently, for **7**-Re, ΔE_{eq}^{v} and ΔG_{eq}° are computed to be quite negative: -10.8 and -6.9 kcal/mol, respectively. The d^6-Os analogue of **7**-Re, on the other hand, is computed to slightly favor terminal N_2 binding (ΔG_{eq}° = +3.6 kcal/mol), which can be attributed to $\Delta BO_{eq}^{\pi} = 0$ in eq 1 due to complete filling of the antibonding $3\pi_\mu^*$ MO of the bridged N_2 complex (entry **7**-Os in Table 5). As found in the octahedral complexes, the r_{MN} bond distances are contracted in the bridged complex of d^5 **7**-Re and stretched in that of d^6 **7**-Os, relative to the corresponding terminal complexes: Δr_{MN} = -0.056 Å and +0.040 Å respectively.

Due to Jahn-Teller effects, the metals in the N_2 complexes of **7**-Re and **7**-Os are in distorted trigonal bipyramidal environments with N_2 trans to an empty coordination site.[45,46] Scheme 8 includes

two fragments with PMe_3 ligands that give five-coordinate N_2 complexes in which the metal is in near idealized trigonal bipyramidal environments (**8**-Fe and **9**-Co). Experimentally, the PEt_3 analog of $[Fe(CO)_2(PMe_3)_2]_2(\mu\text{-}N_2)$ is isolated as a bridging complex with the N_2 ligand in an equatorial position.[47] The crystal structure of $[HCo(PMe_3)_3]_2(\mu\text{-}N_2)$, on the other hand, shows N_2 at an axial position trans to the hydride ligand.[48] Under N_2 atmospheres, both of these complexes equilibrate with the terminal N_2-form, indicating a nearly ergoneutral ΔG°_{eq}. This observation is accord with the above π-bond order model, since the given electronically saturated complexes yield MNNM complexes with $(2\pi_\mu)^4(3\pi^*_\mu)^4$ configurations, resulting in $\Delta BO^{\pi}_{eq} = 0$ for eq 1, with no electronic preference for bridged coordination. The M06L calculations on the N_2 complexes of **8**-Fe and **9**-Co afford ΔG°_{eq} = -0.9 and +3.2 kcal/mol, respectively. For $[HCo(PMe_3)_3]$, an improved agreement with the experiment is achieved using the M06 or B3LYP-D3J functionals, both of which afford ΔG°_{eq} = +1.3 kcal/mol. For comparison we also calculated the N_2 complexes from the d^7-$[HFe(PMe_3)_3]$ fragment (**9**-Fe in eq 8). In this case $HFe(PMe_3)_3(N_2)$ has a square pyramidal geometry with N_2 at a basal position trans to the hydride (eq 8), with one unpaired electron in a σ-type MO having antibonding character with respect to the apical Fe-PMe_3 bond. The given local square pyramidal geometry and electronic structure are largely retained in the d^7-d^7 bridging N_2 complex.

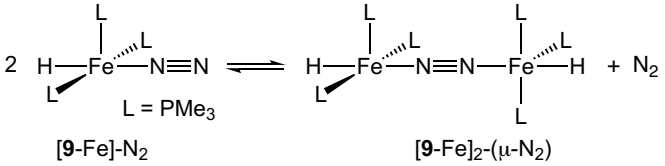

[**9**-Fe]-N_2 $\quad\quad$ [**9**-Fe]$_2$-(μ-N_2) (8)

In spite of the change in the number of d-electrons, therefore, the π-BO in the MNNM core of $[HFe(PMe_3)_3]_2(\mu\text{-}N_2)$ remains the same as in $[HCo(PMe_3)_3]_2(\mu\text{-}N_2)$. As expected, ΔE^{v}_{eq} is computed to be positive in both systems: 4.9 kcal/mol (**9**-Co) vs 8.7 kcal/mol (**9**-Fe), and in both **9**-Co and **9**-Fe the conversion from terminal to bridged coordination is associated with an increase in the M-NN bond distance: Δr_{MN} = 0.031 Å (**9**-Co) and 0.014 Å (**9**-Fe). This result illustrates again how it is the occupancy of the $2\pi_\mu$ and $3\pi^*_\mu$ MOs that controls ΔE^{v}_{eq} and not the geometry or the total number of d electrons or the oxidation state of the metal.

Next, examples of four-coordinate N_2 complexes are considered in Table 5, starting with those derived from Cummins' three-coordinate d^3 molybdenum(III) trigonal planar complex **10**-Mo, the first system ever reported to directly split N_2 into terminal metal nitrides.[49] Exposure of solutions of **10**-Mo to N_2 at low temperatures yields a μ-N_2 product that cleaves upon warming into two metal nitrides. Although the terminal Mo-N_2 complex was proposed as a logical intermediate in the reaction leading to the bridged complex it was never detected, suggesting the fragment has a much greater preference for μ-N_2 binding. Consistently, for **10**-Mo, eq 1 is calculated to be exergonic by 11.6 kcal/mol. The amido ligands in [**10**-Mo]$_2$(μ-N_2) adopt orientations that engage their filled p-orbitals in

π-bonding with the metal (d_{xy},d_{x2-y2}) AOs imparting high antibonding character to the δ_μ MOs. This forces the d^3-d^3 electrons into a $(2\pi_\mu)^4(3\pi_\mu^*)^2$ configuration rather than $(2\pi_\mu)^4(\delta_\mu)^2(3\pi_\mu^*)^0$ as found in the octahedral d^3-d^3 [ᶜ**2**-Ta]$_2$(μ-N_2) in Table 3, for example. Consequently, ΔE_{eq}^{v} is much *less negative* for **10**-Mo, than for ᶜ**2**-Ta (-12.4 vs -25.5 kcal/mol).

Since the systems that bind N_2 most strongly also give ground-state weakening of the N-N bond, it is easy to conflate this with the ability to cleave the N-N bond. As noted, however, ΔE_{eq}^{v} is not particularly negative, for example, for the N_2-splitting complex **10**-Mo as compared with ᶜ**2**-Ta. Furthermore, **10**-Mo forms a bridged dimer in which the N-N bond is shorter (1.203 Å vs. 1.255 Å) and has a much higher N-N stretching frequency (1726 cm^{-1} vs 1457 cm^{-1}) than the N-N bond of [ᶜ**2**-Ta]$_2$(μ-N_2). Importantly, cleavage of the N-N bond by [**10**-Mo]$_2$(μ-N_2) occurs not *in spite* of it having a "stronger" N-N bond than [ᶜ**2**-Ta]$_2$(μ-N_2). Rather, the same factors that lead to this shorter (*less activated*) N-N bond, actually also lead to N-N bond scission. Specifically, the high-energy electrons residing in the $3\pi_\mu^*$ anti-bonding orbital, which has N-N bonding character, subsequently occupy the σ∗ type-MO orbital that is antibonding in NN in the transition state, and ultimately occupy the lone-pair orbitals in the nitride products.[50,51] The requirements for N_2-bridged complexes to split into a pair of metal nitride complexes have been summarized in a recent Perspective article[19].

In the μ-N_2 complex of the d^4-Tc^{III} analog of **10**-Mo, the d^4-d^4 configuration would be $(2\pi_\mu)^4(3\pi_\mu^*)^4$. In this case $3\pi_\mu^*$ is completely filled, so there is no electronic preference for N_2 bridging anymore. Accordingly, for **10**-Tc, eq 1 is computed to have positive ΔE_{eq}^{v} and ΔG_{eq}° values, favoring terminal N_2 coordination (Table 5).

Table 5 includes results on N_2 coordination to two three coordinate-metal fragments bearing tripodal ligands, namely d^7-Fe[$HB^{iPr}P_3$] (**11**-Fe) and d^9-Co[$MeC^{Ph}P_3$] (**12**-Co). Experimentally, the dinitrogen complexes from **12**-Co and the Fe[$PhB^{iPr}P_3$] analogous fragment of **11**-Fe have been isolated in the bridging form.[52,53] The bridging complexes of both **11**-Fe and **12**-Co have and two unpaired electrons in $3\pi_\mu^*$, so they are expected to be favored over the terminal complexes (ΔBO_{eq}^{π} = 1 in eq 1). The increased ΔBO_{eq}^{π} is supported by metal-N_2 bond distances that are shorter in the bridged complexes, and ΔG_{eq}° values that are modestly negative: -3.9 (**11**-Fe) and -5.0 (**12**-Co) kcal/mol. In both cases ΔE_{eq}^{v} is also negative, although only slightly, -1.4 kcal/mol.

The metals in the four-coordinate N_2 complexes covered above are in tetragonal environments. Another class of four-coordinate N_2 complexes in Table 5 is derived from the d^8 T-shaped fragment, **13**-Ir, which affords square planar closed shell products. Under 102 torr N_2 atmosphere, the terminal N_2 complex of **13**-Ir was found to equilibrate in solution with 3% of the bridging N_2 complex, indicating a slightly endergonic ΔG_{eq}°;[54] this is well reproduced by the calculations (ΔG_{eq}° = +1.6 kcal/mol). The calculated ΔE_{eq}^{v} in this system is +2.4 kcal/mol, unsurprisingly since $2\pi_\mu$ and $3\pi_\mu^*$ are

both filled in the μ-N_2 complex. As compared with the octahedral d^6 ^{t}**1**-Mo in Table 1, $\Delta E_2^{\mathrm{int}}$ in **13**-Ir is only -3.4 kcal/mol, which is not sufficiently negative to offset $\Delta E^{\mathrm{v}}_{\mathrm{eq}}$ and favor bridging coordination in **13**-Ir.

The last entry in Table 5 is for a high-spin μ-N_2 complex of the iron(I) β-diketiminate fragment **14**-Fe developed by Holland and co-workers.[55] We calculate the three-coordinate terminal and bridging N_2 complexes of **14**-Fe in the quartet and septet spin states, respectively. The occupancy of the two π-MOs of interest in the septet state is $(2\pi_\mu)^4$ and $(3\pi^*_\mu)^2$. Thus, as per Scheme 5, $\Delta BO^{\pi}_{\mathrm{eq}}$ should be equal to 1. As expected, the computed $\Delta G^{\circ}_{\mathrm{eq}}$ in this system is exergonic: -9.3 kcal/mol and $\Delta E^{\mathrm{v}}_{\mathrm{eq}}$ is negative (-3.3 kcal/mol).

Conclusions and limitations. The difference between the intrinsic strengths of the terminal and bridging M-N_2 bonds $\Delta E^{\mathrm{v}}_{\mathrm{eq}}$ for eq 1 as defined in Scheme 2 is computed to vary between +8.7 and -35.0 kcal/mol per M-N bond in a set of transition metal complexes (Tables 1, 3 and 5). The related free energy values for the equilibrium between a bridged complex plus free N_2 and terminal N_2 complexes vary from +9.1 to -24.0 kcal/mol. If viewed in terms of a given fragment, M, coordinating either to free N_2 or to a coordinated N_2 (MNN unit), this corresponds to differences in the binding free energies ranging from 18.2 kcal/mol favoring coordination of free N_2, to 48.0 kcal/mol favoring the coordination of the MNN unit. This represents a remarkably large range of difference between seemingly similar bonding interactions, 66 kcal/mol, dependent upon the nature of M.

We identify an electronic factor that plays the critical role in determining these trends. The number of π-bonds in the triatomic MNN moiety of a terminal MN_2 complex (BO^{π}_{term}) is 2, i.e. the same as the π-BO of the free N_2 molecule, regardless of the number of electrons supplied by the d-orbitals of the metal to the π_{term}-MOs. In the tetratomic bridging MNNM core, in contrast, the total number of π-bonds, BO^{π}_{μ}, can be 2, 3 or 4, depending on the occupancy of the bonding and antibonding π_μ-MOs. Based on the number of π-bonds alone, bridging coordination is expected to be more favored over terminal coordination when $BO^{\pi}_{\mu} = 3$ or 4, but not when $BO^{\pi}_{\mu} = 2$. As illustrated in Scheme 9, all that is needed to apply this model is knowledge of the number of d-electrons supplied by the two metals to the π-manifold of MNNM (d^n_π-d^n_π) as these define the occupancy of the bonding $2\pi_\mu$ and antibonding $3\pi^*_\mu$ MOs of the bridging complex. In this work, DFT methods were employed to identify the orbital occupancy and develop quantitative MO diagrams. In principle, however, a qualitative MO diagram could provide valuable predictions about the $\Delta BO^{\pi}_{\mathrm{eq}}$ value and thus the propensity to form a bridging or terminal complex under nitrogen.

Scheme 9. Number of π-bonds (BO^{π}) in terminal and bridging N_2 complexes, and change in total BO^{π} upon bridge formation

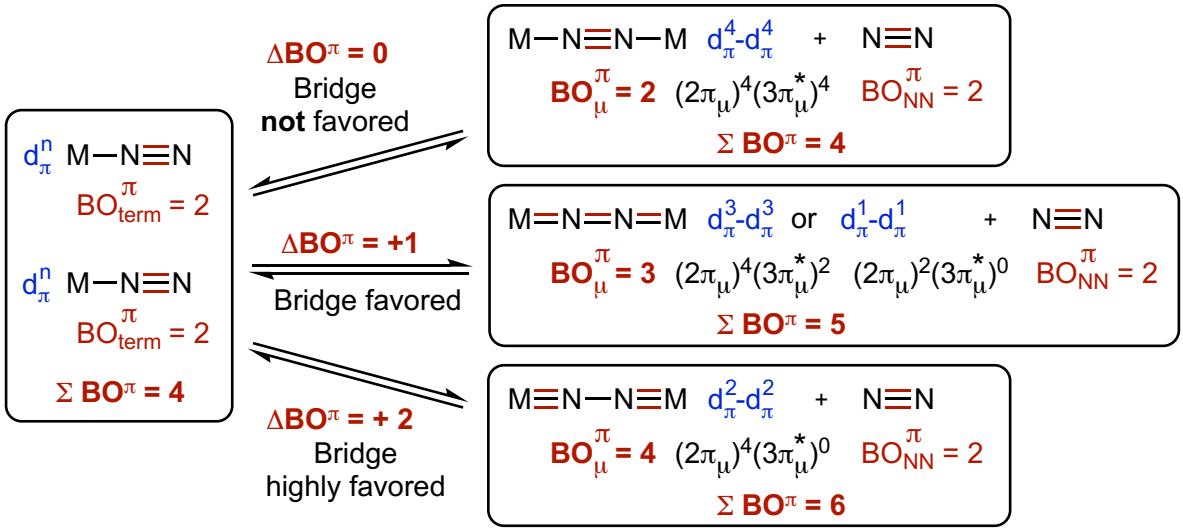

For d_{π}^{4}-d_{π}^{4} systems, as encountered in 18-electron and d^8 square planar terminal-N_2 complexes, the full π-electron configuration in MNNM (including the four π-electrons from N_2) is $(1\pi_{\mu})^4(2\pi_{\mu})^4(3\pi_{\mu}^{*})^4$. Thus $BO_{\mu}^{\pi} = 2$, so the interconversion of two terminal MNN complexes to MNNM and free N_2 is not associated with any change in the number of π-bonds: $\Delta BO_{eq}^{\pi} = 0$. The terminal M-NN bonds in these systems are computed to be intrinsically stronger than the bridging ones, yielding positive ΔE_{eq}^{v} values for eq 1. However, the calculations show that outer-sphere dispersion interactions between the ligands of the two metal fragments can mitigate the effects of ΔE_{eq}^{v}, and can even favor bridging coordination in some d_{π}^{4}-d_{π}^{4} cases. It is therefore no surprise that, experimentally, many electronically saturated complexes exist in solution under N_2 as a mixture of the terminal and bridging forms. In d_{π}^{3}-d_{π}^{3} systems, the partial occupancy of $3\pi_{\mu}^{*}$ relative to the d_{π}^{4}-d_{π}^{4} systems leads to $BO_{\mu}^{\pi} = 3$. In this case, converting two MNN to MNNM and N_2 results in the creation of an additional π-bond ($\Delta BO_{eq}^{\pi} = 1$), which is expected to directly favor bridging over terminal coordination. Naturally, an even greater preference for bridging is reached in the d_{π}^{2}-d_{π}^{2} systems ($\Delta BO_{eq}^{\pi} = 2$), and these are computed to have highly negative values of ΔE_{eq}^{v}, reaching -35.0 kcal/mol. Finally, a d_{π}^{1}-d_{π}^{1} MNNM core would again offer $\Delta BO_{eq}^{\pi} = 1$. Interestingly, based on crystallographic data, μ-N_2 complexes are often shown using varied Lewis structures, including: M-N≡N-M, M=N=N=M and M≡N-N≡M. When inspected side by side, it becomes evident that the given structures reflect different total numbers of π-bonds (2, 3, and 4, respectively) rather than resonance structures of the same number of π-bonds, as in the M-N≡N ↔ M=N=N pair, for example.

Scheme 9 can be used to explain in a general way the dependence of ν_{NN}, the geometric parameters, and ΔE_{eq}^{v} on the π-electron configuration of MNNM. The ν_{NN} of MNNM varies from

1457 cm^{-1} to 2173 cm^{-1}, and correlates strongly with ΔE^{v}_{eq} (Fig. S1). In contrast, values of ν_{NN} of the terminal M-NN complexes vary only in a narrow range, 1962 to 2184 cm^{-1}, reflecting the non-bonding nature of the $2\pi_{term}$ orbitals with respect to the N-N bond, and ν_{NN} does not correlate with ΔE^{v}_{eq} (Fig. S5). A qualitative π-MO diagram for MNNM similar to the one in Fig. 1A was first adopted by Chatt and Richard to account for the trends in NN stretching vibrational frequency (ν_{NN}) observed when the octahedral terminal N_2 complex *trans*-$Cl(PMe_2Ph)_4Re(N_2)$ is bridged to other five-coordinate transition metal fragments with varied d-electron counts.[56] Related schemes have since been adapted in several studies focused on the degree of N_2 activation in bridging complexes.[57,58]

There are limitations to the proposed model. First, this model intentionally focuses on counting the change in the number of π-bonds in eq 1 (ΔBO^{π}_{eq}) and does not address the variation in the strength of the individual bonds (σ and π) which is undoubtedly relevant for quantitative purposes. For example, the MNN BO^{π}_{term} of octahedral d^5 and d^6 terminal complexes is noted to be formally the same, yet the vertical dissociation energy of N_2 ($-\Delta E^{v}_{1}$) in related complexes is systematically greater for the d^6 complexes. On the other hand, the MNNM BO^{π}_{μ} is greater in the octahedral d^5-d^5 systems than the d^6-d^6 ones, yet for analogous pairs of complexes the vertical dissociation energies ($-\Delta E^{v}_{2}$) are computed to be comparable. Likewise, although the ΔBO^{π}_{eq} term readily separates the ΔE^{v}_{eq} values in the octahedral complexes into three non-overlapping sets (slightly positive, modestly negative, and highly negative), the variations within each set are still substantial, reaching near 10 kcal/mol when ΔBO^{π}_{eq} = 1 or 2. Finally, in some tetragonal complexes of the first row metals with ΔBO^{π}_{eq} = 1, ΔE^{v}_{eq} is only slightly negative. This may not be too surprising since the attributes of the metal, such as the effective nuclear charge, electronegativity, size and oxidation state, as well as the nature of the ligands, can all play important roles in affecting both the σ- and π- components of the coordination energies, but are absent from the simple model considering only the number of the formal π-bonds. Second, changes in the spin states and the dispersion interactions from the left to the right side of eq 1 can influence ΔG°_{eq}. We have factored out the effects of these factors via the ΔE^{dist}_{1}, ΔE^{dist}_{2} and ΔE^{int}_{2} terms in Scheme 3. In an extreme case, for example, sufficiently bulky ligands can prevent bridging that would be otherwise favorable.

Even with its potential limitations, counting the π-bonds provides a simple and rapid way to obtain rough estimates of the preference of different fragments for terminal or bridging N_2 coordination. The π-BO model should be also applicable to understand the stability of N_2-bridged heterobimetallic complexes and complexes with odd number of d^m_π-d^n_π π-electrons leading to non-integer BO^{π}_{μ} values. The binding mode adopted by a metal has important ramifications on which mechanistic pathways for N_2 activation and functionalization are available. Understanding the factors that control the different binding modes may help guide the choice of metal-ligand combinations to investigate for catalytic transformations of N_2.

Computational Methods DFT calculations were performed using the M06-L functional as implemented in *Gaussian-16*.[59] The suitability of this functional to estimate the energies of organometallic reactions has been validated in several studies.[60,61] Geometry optimization and harmonic normal mode vibrational analyses were carried out in the gas phase using the 6-311G(d,p) basis set on the main group elements and the first row transition metals.[62,63,64] The heavier metals carried the SDD relativistic effective core potentials (ECP) and associated basis sets,[65] and were augmented with one additional polarization *f*-function from the Frenking basis set.[66] The thermal and entropy terms to the Gibbs free energy were computed at 298 K with N_2 at a pressure of 1 atm and the metal complexes adjusted to 1 M concentrations.[67,68] Final energies were obtained from single point calculations in a polarizable continuum[69] representing toluene as solvent using the gas phase geometries and the def2-tzvp basis set implemented in Gaussian on the non-metals, and the def2-qzvp with associated ECPs as provided on the Basis Set Exchange website on the heavier metals.[70,71,] The given computational model gives $\Delta G^{\circ}_{\mathrm{eq}}$ = 1.6 kcal/mol for the equilibrium between the terminal and bridging N_2 complexes of the ($^{\mathrm{tBu}}$PCP)Ir fragment **13**-Ir (Table 5). This result is in satisfactory agreement with the observation of an equilibrium between the two bridging modes in solution under an atmosphere of N_2. Some energies were also computed using few other popular density functionals for comparison. We find that $\Delta G^{\circ}_{\mathrm{eq}}$ is not greatly sensitive to the level of theory as long as dispersion interactions are included. For example, at the M06, ωB97X-D, B3LYP and B3LYP-D3 levels, $\Delta G^{\circ}_{\mathrm{eq}}$ for the N_2 complexes of **13**-Ir are: 0.3, -2.6, 11.2 and 0.9 kcal/mol, respectively. Even smaller variations are obtained at these levels for $\Delta E^{\mathrm{v}}_{\mathrm{eq}}$, namely: 2.4 (M06-L), 1.9 (M06), 1.9 (ωB97XD), 1.8 (B3LYP), and 2.6 (B3LYP-D3J); in kcal/mol. These results for **13**-Ir show the M06-L level to be satisfactory to study the trends in $\Delta G^{\circ}_{\mathrm{eq}}$ and $\Delta E^{\mathrm{v}}_{\mathrm{eq}}$ of interest to the present study. We note, though, that the M06L level appears to exaggerate the individual N_2 coordination energies to the fragment compared to the other levels.

Author Information
Corresponding Authors
Faraj Hasanayn - *Department of Chemistry, American University of Beirut, Beirut 1107 2020, Lebanon*;
ORCID http://orcid.org/0000-0003-3308-7854; Email: fh19@aub.edu.lb

Patrick L. Holland - *Department of Chemistry, Yale University, New Haven, Connecticut 06520, United States*;
ORCID http://orcid.org/0000-0002-2883-2031; Email: patrick.holland@yale.edu

Alexander J. M. Miller - *Department of Chemistry, University of North Carolina at Chapel Hill, Chapel Hill, North Carolina 27599-3290, United States*;
ORCID http://orcid.org/0000-0001-9390-3951; Email: ajmm@email.unc.edu

Alan S. Goldman - *Department of Chemistry and Chemical Biology, Rutgers, The State University of New Jersey, New Brunswick, New Jersey 08903, United States*;
ORCID http://orcid.org/0000-0002-2774-710X; Email: alan.goldman@rutgers.edu

Authors

Lynn S. Yamout - *Department of Chemistry, American University of Beirut, Beirut 1107 2020, Lebanon;*
ORCID https://orcid.org/0000-0002-7008-4866 ; Email: lmy02@mail.aub.edu

Mohamad Ataya - *Department of Chemistry, American University of Beirut, Beirut 1107 2020, Lebanon;*
ORCID http://orcid.org/0000-0002-5050-9724 ; Email: maa190@mail.aub.edu

Notes The authors declare no competing financial interest.

Acknowledgements

This work was supported through the NSF Chemical Catalysis program under Grant Nos. CHE-1954254, CHE-1954942, and CHE-1955014. Additional support was provided from LNCSR-AUB. Computer resources were provided by the HPC centers at AUB and Rutgers University.

Supporting Information Statement

Absolute Energies, MO displays, and plots of ΔE_{eq}^{v} against ν_{NN} (pdf). Coordinates of the optimized geometries (xyz.txt and mol2.txt).

References

(1) Allen, A. D.; Senoff, C. W. Nitrogenopentammineruthenium(II) Complexes. *Chem. Commun.* **1965**, 621-622.

(2) (a) Dilworth, J. R.; Richards, R. L. Reactions of Dinitrogen Promoted by Transition Metal Complexes; Wilkinson, G., Stone, F. G. A., Abel, E. W., Ed.; Pergamon Press: Oxford, 1982; Vol. 8, p 1073. (b) Hidai, M.; Mizobe, Y. Reactions of coordinated dinitrogen and related species; Braterman, P. S., Ed.; Plenum Press: New York, 1989; Vol. 2, p 53-114. (c) Hidai, M.; Mizobe, Y. Recent Advances in the Chemistry of Dinitrogen Complexes. *Chem. Rev.* **1995**, *95*, 1115-1133. (d) MacLeod, C.; Holland, P. L. Recent Developments in Homogeneous Dinitrogen Reduction by Molybdenum and Iron. *Nat. Chem.* **2013**, *5*, 559-565.

(3) (a) Postgate, J. Nitrogen Fixation, 3rd ed.; Cambridge University Press: Cambridge, U.K., 1998. (b) Schlögl, R. Catalytic Synthesis of Ammonia: A "Never-Ending Story"? *Angew. Chem. Int. Ed.* **2003**, *42*, 2004-2008.

(4) (a) Pickett, C. J.; Talarmin, J. Electrosynthesis of Ammonia. *Nature* **1985**, *317*, 652-653. (b) Kyriakou, V.; Garagounis, I.; Vasileiou, E.; Vourros, A.; Stoukides, M. Progress in the Electrochemical Synthesis of Ammonia. *Catal. Today* **2017**, *286*, 2-13.

(5) Hochman, G.; Goldman, A. S.; Felder, F. A.; Mayer, J. M.; Miller, A. J. M.; Holland, P. L.; Goldman, L. A.; Manocha, P.; Song, Z.; Aleti, S. Potential Economic Feasibility of Direct Electrochemical Nitrogen Reduction as a Route to Ammonia. *ACS Sustain. Chem. Eng.* **2020**, *8*, 8938–8948.

(6) (a) Chalkley, M. J.; Drover, M. W.; Peters, J. C. Catalytic N_2-to-NH_3 (or -N_2H_4) Conversion by Well-Defined Molecular Coordination Complexes. *Chem. Rev.* **2020**, *120*, 5582–5636. (b) Roux, Y.; Duboc, C.; Gennari, M. Molecular Catalysts for N_2 Reduction: State of the Art, Mechanism, and Challenges. *ChemPhysChem* **2017**, *18*, 2606 – 2617.

(7) (a) Harrison, D. F.; Weissberger, E.; Taube, H. Binuclear Ion Containing Nitrogen as a Bridging Group. *Science* **1968**, *159*, 320-322. (b) Chatt, J.; Dilworth, J. R.; Richards, R. Recent Advances in the Chemistry of Nitrogen Fixation. *Chem. Rev.* **1978***, 78*, 589-626.

(8) (a) Fryzuk, M. D.; Johnson, S. A.; Patrick, B. O.; Albinati, A.; Mason, S. A.; Koetzle, T. F. New Mode of Coordination for the Dinitrogen Ligand: Formation, Bonding, and Reactivity of a Tantalum Complex with a Bridging N_2 Unit That Is Both Side-On and End-On. *J. Am. Chem. Soc.* **2001**, *123*, 3960-3973. (b) Fryzuk, M. D. Side-on End-on Bound Dinitrogen: An Activated Bonding Mode That Facilitates Functionalizing Molecular Nitrogen. *Acc. Chem. Res.* **2003**, *42*, 127-133.

(9) Sorsche, D.; Miehlich,M. E.; Searles, K.; Gouget, G.; Zolnhofer, E. M.; Fortier, S.; Chen, C.-H.; Gau, M.; Carroll, P. J.; Murray, C. B.; Caulton, K. G.; Khusniyarov, M. M.; Meyer, K.; Mindiola, D. J. Unusual Dinitrogen Binding and Electron Storage in Dinuclear Iron Complexes. *J. Am. Chem. Soc.* **2020**, *142*, 8147-8159.

(10) Holland, P. L. Metal-dioxygen and metal-dinitrogen complexes: where are the electrons? *Dalton Transactions* **2010**, *39*, 5415-5425.

(11) Side-on bridging N_2 complexes (μ-η^2:η^2-N_2) are known, but their consideration is beyond the scope of the present study.

(12) (a) Burford, R. J.; Fryzuk, M. D. Examining the Relationship between Coordination Mode and Reactivity of Dinitrogen. *Nat. Rev. Chem.* **2017**, *1*, 0026. (b) MacKay, B. A.; Fryzuk, M. D. Dinitrogen Coordination Chemistry: On the Biomimetic Borderlands. *Chem. Rev.* **2004**, *104*, 385-401.

(13) Khoenkhoen, N.; de Bruin, B.; Reek, J. N. H.; Dzik, W. I. Reactivity of Dinitrogen Bound to Mid- and Late-Transition-Metal Centers. *Eur. J. Inorg. Chem.* **2015**, *2015*, 567-598.

(14) Masero, F.; Perrin, M. A.; Dey, S.; Mougel, V. Dinitrogen Fixation: Rationalizing Strategies Utilizing Molecular Complexes. *Chem. Eur. J.* **2020**, *26*, 13383-13389.

(15) Kim, S.; Loose, F.; Chirik, P. J. Beyond Ammonia: Nitrogen-Element Bond Forming Reactions with Coordinated Dinitrogen. *Chem. Rev.* **2020**, *120*, 5637-5681.

(16) Chatt, J.; Pearman, A. J.; Richards, R. L. The Reduction of Mono-Coordinated Molecular Nitrogen to Ammonia in a Protic Environment. *Nature* **1975**, *253*, 39-40.

(17) (a) Yandulov, D. V.; Schrock, R. R. Catalytic Reduction of Dinitrogen to Ammonia at a Single Molybdenum Center. *Science* **2003**, *301*, 76-78. (b) Weare, W. W.; Dai, X.; Byrnes, M. J.; Chin, J. M.; Schrock, R. R.; Müller, P. Catalytic reduction of dinitrogen to ammonia at a single molybdenum center. *Proc. Nat. Ac. Sci.* **2006**, *103*, 17099-17106. (c) Yandulov, D. V.; Schrock, R. R. Reduction of Dinitrogen to Ammonia at a Well-Protected Reaction Site in a Molybdenum Triamidoamine Complex *J. Am. Chem. Soc.* **2002**, *124*, 6252–6253. (d) Yandulov, D. V.; Schrock, R. R. Studies Relevant to Catalytic Reduction of Dinitrogen to Ammonia by Molybdenum Triamidoamine Complexes *Inorg. Chem.* **2005**, *44*, 1103–1117.

(18) Klopsch, I.; Yuzik-Klimova, E. Y.; Schneider, S. Functionalization of N_2 by Mid to Late Transition Metals via N–N Bond Cleavage; Nishibayashi, Y., Ed.; Springer: Cham, 2017; pp 71-112.

(19) Bruch, Q. J.; Connor, G. P.; McMillion, N. D.; Goldman, A. S.; Hasanayn, F.; Holland, P. L.; Miller, A. J. M. Considering Electrocatalytic Ammonia Synthesis via Bimetallic Dinitrogen Cleavage. *ACS Catal.* **2020**, *10*, 10826-10846.

(20) Ashida, Y.; Arashiba, K.; Nakajima, K.; Nishibayashi, Y. Molybdenum-Catalysed Ammonia Production with Samarium Diiodide and Alcohols or Water. *Nature* **2019**, *568*, 536–540.

(21) Dunn, P. L.; Cook, B. J.; Johnson, S. I.; Appel, A. M.; Bullock, M. R. Oxidation of Ammonia with Molecular Complexes. *J. Am. Chem. Soc.* **2020**, *142*, 17845−17858.

(22) Valera-Medina, A.; Amer-Hatem, F.; Azad, A. K.; Dedoussi, I. C.; de Joannon, M.; Fernandes, R. X.; Glarborg, P.; Hashemi, H.; He, X.; Mashruk, S.; McGowan, J.; Mounaim-Rouselle, C.; Ortiz-Prado, A.; Ortiz-Valera, A.; Rossetti, I.; Shu, B.; Yehia, M.; Xiao, H.; Costa, M. Review on Ammonia as a Potential Fuel: From Synthesis to Economics. *Energy Fuels* **2021**, *35*, 6964-7029.

(23) Wasada-Tsutsui, Y.; Wasada, H.; Suzuki, T.; Katayama, A.; Kajita, Y.; Inomata, T.; Ozawa, T.; Masuda, H. Efficient Electronic Structure to Stabilize N_2-Bridged Dinuclear Complexes Intended for N_2 Activation: Iminophosphorane Iron(I) and Cobalt(I). *Eur. J. Inorg. Chem.* **2020**, 1411-1417.

(24) Zhao, Y.; Truhlar, D. G. A new local density functional for main-group thermochemistry, transition metal bonding, thermochemical kinetics, and noncovalent interactions. *J. Chem. Phys.* **2006**, *125*, 194101-194118.

(25) (a) Arashiba, K.; Miyake, Y.; Nishibayashi, Y. A Molybdenum Complex Bearing PNP-Type Pincer Ligands Leads to the Catalytic Reduction of Dinitrogen into Ammonia. *Nat. Chem.* **2011**, *3*, 120-125. (b) Kuriyama, S.; Arashiba, K.; Nakajima, K.; Tanaka, H.; Kamaru, N.; Yoshizawa, K.; Nishibayashi, Y. Catalytic Formation of Ammonia from Molecular Dinitrogen by Use of Dinitrogen-Bridged Dimolybdenum–Dinitrogen Complexes Bearing PNP-Pincer Ligands: Remarkable Effect of Substituent at PNP-Pincer Ligand. *J. Am. Chem. Soc.* **2014**, *136*, 9719-9731. (c) Tanaka, H.; Nishibayashi, Y.; Yoshizawa, K. Interplay between Theory and Experiment for Ammonia Synthesis Catalyzed by Transition Metal Complexes. *Acc. Chem. Res.* **2016**, *49*, 987-995.

(26) Zhao, Y.; Truhlar, D. Attractive Noncovalent Interactions in the Mechanism of Grubbs Second-Generation Ru Catalysts for Olefin Metathesis. *Org. Lett.* **2007**, *9*, 1967-1970.

(27) (a) Becke, A. D. Density-functional thermochemistry III. The role of exact exchange *J. Chem. Phys.* **1993**, *98*, 5648-5652. (b) Lee, C.; Yang, W.; Parr, R. G. Development of the Colle-Salvetti correlation-energy formula into a functional of the electron density. *Phys. Rev. B* **1988**, *37*, 785-789.

(28) Grimme, S.; Ehrlich, S.; Goerigk, L. Effect of the damping function in dispersion corrected density functional theory. *J. Comput. Chem.* **2011***, 32*, 1456-1465.

(29) Becke, A. D.; Johnson, E. R. A density-functional model of the dispersion interaction. *J. Chem. Phys.* **2005**, *123*, 154101-154109.

(30) Liptrot, D. J.; Power, P. P. London dispersion forces in sterically crowded inorganic and organometallic molecules. *Nat. Rev. Chem.* **2017**, *1*, 0004.

(31) Bruch, Q. J.; Connor, G. P.; Chen, C.-H.; Holland, P. L.; Mayer, J. M.; Hasanayn, F.; Miller, A. J. M. Dinitrogen Reduction to Ammonium at Rhenium Utilizing Light and Proton-Coupled Electron Transfer. *J. Am. Chem. Soc.* **2019**, *141*, 20198-20208.

(32) Schendzielorz, F.; Finger, M.; Abbenseth, J.; Würtele, C.; Krewald, V.; Schneider, S. Metal-Ligand Cooperative Synthesis of Benzonitrile by Electrochemical Reduction and Photolytic Splitting of Dinitrogen. *Angew. Chem. Int. Ed.* **2019**, *58*, 830–834.

(33) (a) Bezdek, M. J.; Guo, S.; Chirik, P. J. Terpyridine Molybdenum Dinitrogen Chemistry: Synthesis of Dinitrogen Complexes That Vary by Five Oxidation States. *Inorg. Chem.* **2016**, *55*, 3117-3127. (b) Schendzielorz, F.; Finger, M.; Abbenseth, J.; Würtele, C.; Krewald, V.; Schneider, S. Metal-Ligand Cooperative Synthesis of Benzonitrile by Electrochemical Reduction and Photolytic Splitting of Dinitrogen. *Angew. Chem. Int. Ed.* **2019**, *58*, 830-834. (c) Rupp, S.; Plasser, F.; Krewald, V. Multi-Tier Electronic Structure Analysis of Sita's Mo and W Complexes Capable of Thermal or Photochemical N_2 Splitting. *Eur. J. Inorg. Chem.* **2020**, *2020*, 1506-1518.

(34) (a) Cotton, A. F. Chemical Applications of Group Theory, 3rd Ed. 1990. Wiley. John Wiley & Sons, Inc., NY. (b) Albright, T. A.; Burdett, J. K.; Whangbo, M-H; Orbital Interactions in Chemistry, 2nd Ed. 2013. John Wiley & Sons, Inc. Hoboken, NJ.

(35) DuBois, D. L.; Hoffmann, R. Diazenido, Dinitrogen and Related Complexes. *Nouv. J. Chim.* **1977***, 1,* 479-492.

(36) The given closed singlet state is computed to be 8.5 kcal/mol lower in energy than the quintet spin state of from the $(1\pi_\mu)^4(2\pi_\mu)^2(3\pi_\mu^*)^2$ configuration, which was observed in a different system. See next reference.

(37) Silantyev, G. A.; Förster, M.; Schluschaß, B.; Abbenseth, J.; Würtele, C.; Volkmann, C.; Holthausen, M. C.; Schneider, S., Dinitrogen Splitting Coupled to Protonation. *Angew. Chem., Int. Ed*. **2017**, *56*, 5872-5876.

(38) Caselli, A.; Solari, E.; Scopelliti, R.; Floriani, C.; Re, N.; Rizzoli, C.; Chiesi-Villa, A. Dinitrogen Rearranging over a Metal−Oxo Surface and Cleaving to Nitride: From the End-On to the Side-On Bonding Mode, to the Stepwise Cleavage of the N⁝N Bonds Assisted by NbIII-Calix[4]Arene. *J. Am. Chem. Soc.* **2000**, *122*, 3652-3670.

(39) Turner, H. W.; Fellmann, J. D.; Rocklage, S. M.; Schrock, R. R.; Churchill, M. R.; Wasserman, H. J. Tantalum Complexes Containing Diimido Bridging Dinitrogen Ligands. *J. Am. Chem. Soc.* **1980**, *102*, 7809-7811.

(40) Kilgore, U. J.; Yang, X.; Tomaszewski, J.; Huffman, J. C.; Mindiola, D. J. Activation of Atmospheric Nitrogen and Azobenzene N=N Bond Cleavage by a Transient Nb(III) Complex. *Inorg. Chem.* **2006**, *45*, 10712-10721.

(41) Klopsch, I.; Finger, M.; Würtele, C.; Milde, B.; Werz, D. B.; Schneider, S. Dinitrogen Splitting and Functionalization in the Coordination Sphere of Rhenium. *J. Am. Chem. Soc.* **2014**, *136*, 6881-6883.

(42) Lindley, B. M.; van Alten, R. S.; Finger, M.; Schendzielorz, F.; Würtele, C.; Miller, A. J. M.; Siewert, I.; Schneider, S. Mechanism of Chemical and Electrochemical N_2 Splitting by a Rhenium Pincer Complex. *J. Am. Chem. Soc.* **2018**, *140*, 7922–7935.

(43) Besmer, M. C.; Braband, H.; Schneider, S.; Spingler, B.; Alberto, R. Exploring the Coordination Chemistry of N_2 with Technetium PNP Pincer-Type Complexes, *Inorg. Chem.* **2021**, *60*, 6696-6701.

(44) Tsvetkov, N.; Fan, H.; Caulton, K. G. An evaluation of monovalent osmium supported by the PNP ligand environment. *Dalton Trans.* **2011**, *40*, 1105-1110.

(45) Bersuker, I. B. Modern Aspects of the Jahn-Teller Effect: Theory and Applications To Molecular Problems *Chem. Rev.* **2001**, *101*, 1067-1114.

(46) (a) Rachidi, I. E.; Eisenstein, O.; Jean, Y. A theoretical study of the possible structures of d^6 ML_5 complexes. *New J. Chem.* **1990**, *14*, 671−677. (b) Baroudi, A.; El-Hellani A.; Bengali, A. A.; Goldman, A. S.; Hasanayn, F. Calculation of Ionization Energy, Electron Affinity, and Hydride Affinity Trends in Pincer-Ligated d^8-Ir(^{tBu4}PXCXP) Complexes: Implications for the Thermodynamics of Oxidative H_2 Addition. *Inorg. Chem.* **2014**, *53*, 12348–12359.

(47) Kandler, H.; Gauss, C.; Bidell, W.; Rosenberger, S.; Burgi, T.; Eremenko, I. L.; Veghini, D.; Orama, O.; Burger, P.; Berke, H. The Reduction of $[Fe(CO)_2L_2X_2]$ (L = $P(OMe)_3$, $P(OiPr)_3$, PEt_3; X = Br, I) From Iron(II) to Iron(0) via Stable Iron(I) Intermediates. *Chem. Eur. J.* **1995**, *1*, 541-548.

(48) Klein, H-F.; Beck, H.; Hammerschmitt, G.; Koch, U.; Koppert, S.; Cordier, G.; Paulus, H. Synthesis, Properties, and Structure of a Dinitrogen Bridged Dinuclear Hydridocobalt Complex and its Reactions with 1-Alkynes. *Verlag der Zeitschrift für Naturforschung B* **1991**, *46*, 147-156.

(49) Laplaza, C. E.; Cummins, C. C. Dinitrogen Cleavage by a Three-Coordinate Molybdenum(III) Complex. *Science* **1995**, *268*, 861-863.

(50) Laplaza, C. E.; Johnson, M. J. A.; Peters, J. C.; Odom, A. L.; Kim, E.; Cummins, C. C.; George, G. N.; Pickering, I. J. Dinitrogen Cleavage by Three-Coordinate Molybdenum(III) Complexes: Mechanistic and Structural Data. *J. Am. Chem. Soc.* **1996**, *118*, 8623–8638.

(51) Cui, Q.; Musaev, D. G.; Svensson, M.; Sieber, S.; Morokuma, K. N_2 Cleavage by Three-Coordinate Group 6 Complexes. W(III) Complexes Would Be Better Than Mo(III) Complexes. *J. Am. Chem. Soc.* **1995**, *117*, 12366−12367.

(52) (a) Betley, T. A.; Peters, J. C. Dinitrogen Chemistry from Trigonally Coordinated Iron and Cobalt Platforms. *J. Am. Chem. Soc.* **2003**, *125*, 10782-10783. (b) Betley, T. A.; Peters, J. C. Tetrahedrally Coordinated $L_3Fe\text{-}N_x$ Platform that Accommodates Terminal Nitride ($Fe^{IV}\equiv N$) and Dinitrogen ($Fe^{I}\text{-}N_2\text{-}Fe^{I}$) Ligands *J. Am. Chem. Soc.* **2004**, *126*, 6252-6254.

(53) Cecconi, C.; Ghilardi, C. A.; Midollini, S.; Moneti, S.; Orlandini, A.; Baccib. M. Synthesis, Characterization, and Crystal Structure of the Dimeric, Paramagnetic Cobalt(0) Complex $\{[MeC(CH_2PPh_2)_3Co]_2(\mu\text{-}N_2)\}$. *J. Chem. Soc. Chem. Comm.* **1985**, *11*, 731-733.

(54) Ghosh, R.; Kanzelberger, M.; Emge, T. J.; Hall, G. S.; Goldman, A. S. Dinitrogen Complexes of Pincer-Ligated Iridium. *Organometallics* **2006**, *25*, 5668-5671.

(55) (a) Smith, J. M.; Lachicotte, R. J.; Pittard, K. A.; Cundari, T. R.; Lukat-Rodgers, G.; Rodgers, K. R.; Holland, P. L. Stepwise Reduction of Dinitrogen Bond Order by a Low-Coordinate Iron Complex. *J. Am. Chem. Soc.* **2001**, *123*, 9222-9223. (b) McWilliams, S. F.; Rodgers, K. R.; Lukat-Rodgers, G.; Mercado, B. Q.; Grubel, K.; Holland, P. L. Alkali Metal Variation and Twisting of the FeNNFe Core in Bridging Diiron Dinitrogen Complexes. *Inorg. Chem.* **2016**, *55*, 2960-2968. (c) McWilliams, S. F.; Bunting, P. C.; Kathiresan, V.; Mercado, B. Q.; Hoffman, B. M.; Long, J. R.; Holland, P. L. Isolation and Characterization of a High-Spin Mixed-Valent Iron Dinitrogen Complex. *Chem. Commun.* **2018**, *54*, 13339-13342.

(56) Chatt, J.; Fay, R. C.; Richards, R. L. Preparation and Characterisation of the Dinuclear Dinitrogen Complex, Trichloro-μ-Dinitrogen-Bis(Tetrahydrofuran){chlorotetrakis[Dimethyl-(Phenyl)Phosphine]Rhenium(I)}chromium(III). *J. Chem. Soc. A* **1971**, 702-704.

(57) (a) Re, N.; Rosi, M.; Sgamellotti, A.; Floriani, C. Theoretical Study of Dinitrogen Activation in Dinuclear V(II) and V(III) Hexacoordinated Complexes: Ab Initio Calculations on Various Model Compounds. *Inorg. Chem.* **1995**, *34*, 3410. (b) Ferguson, R.; Solari, E.; Floriani, C.; Osella, D.; Ravera, M.; Re, N.; Chiesi-Villa, A.; Rizzoli, C. Stepwise Reduction of Dinitrogen Occurring on a Divanadium Model Compound: A Synthetic, Structural, Magnetic, Electrochemical, and Theoretical Investigation on the $[V{=}N{=}N{=}V]^{n+}$ [n = 4-6] Based Complexes *J. Am. Chem. Soc.* **1997**, *119*, 10104-10115.

(58) Curley, J. J.; Cook, T. R.; Reece, S. Y.; Müller, P.; Cummins, C. C. Shining Light on Dinitrogen Cleavage: Structural Features, Redox Chemistry, and Photochemistry of the Key Intermediate Bridging Dinitrogen Complex. *J. Am. Chem. Soc.* **2008**, *130*, 9394–9405.

(59) Gaussian 16, Revision D.01. Frisch, M. J. et. al. Gaussian, Inc., Wallingford CT, 2016.

(60) Zhaou, Y.; Truhlar. D. G. Density Functionals with Broad Applicability in Chemistry. *Acc. Chem. Res.* **2008**, *41*, 157-167.

(61) (a) Minenkov, Y.; Singstad, Å.; Occhipinti, G.; Jensen, V. R. The accuracy of DFT-optimized geometries of functional transition metal compounds: a validation study of catalysts for olefin metathesis and other reactions in the homogeneous phase. *Dalton Trans.* **2012**, *41*, 5526-5541. (b) Raju, R. K.; Bengali, A. A., Brothers, E. N. A unified set of experimental organometallic data used to evaluate modern theoretical methods. *Dalton Trans.* **2016**, *45*, 13766-13778. (c) Gusev, D. G. Assessing the accuracy of M06-L organometallic thermochemistry. *Organometallics* **2013**, *32*, 4239-4243.

(62) Raghavachari, K.; Binkley, J. S.; Seeger, R.; Pople, J. A. Self-Consistent Molecular Orbital Methods. 20. Basis set for correlated wave-functions. *J. Chem. Phys.* **1980**, *72*, 650-654.

(63) McLean, A. D.; Chandler, G. S. Contracted Gaussian basis sets for molecular calculations. I. Second row atoms, Z = 11–18. *J. Chem. Phys.* **1980**, 72, 5639-5648.

(64) Rassolov, V. A., Pople, J. A., Ratner, M. A., Windus, T. L. 6-31G* basis set for atoms K through Zn. *J. Chem. Phys.* **1998**, *109*, 1223-1229.

(65) Andrae, D.; Häußermann, U.; Dolg, M.; Stoll, H.; Preuss, H. Energy-adjusted *ab initio* pseudopotentials for the second and third row transition elements. *Theor. Chim. Acta.* **1990**, *77*, 123-141.

(66) Ehlers, A. W.; Böhlers, A. W.; Bohme, M.; Dapprich, S.; Gobbi, A.; Höllwarth, A.; Jonas, V.; Köhler, K. F.; Stegmann, R.; Veldkamp, A.; Frenking, G. A set of f-polarization Functions for Pseudo-Potential Basis Sets of the Transition Metals Sc-Cu, Y-Ag and La-Au *Chem. Phys. Lett.* **1993**, *208*, 111–114.

(67) Cramer, C. J. Essentials of Computational Chemistry: Theories and Models, 2nd ed.; Wiley, 2004.

(68) Jensen, H. I. Predicting accurate absolute binding energies in aqueous solution: thermodynamic considerations for electronic structure methods. *Phys.Chem.Chem.Phys.* **2015**, *17*, 12441-12451.

(69) Marenich, A, V.; Cramer, C. J.; Truhlar, C. J. Universal solvation model based on solute electron density and on a continuum model of the solvent defined by the bulk dielectric constant and atomic surface tensions. *J. Phys. Chem. B* **2009**, *113*, 6378-6396.

(70) (a) Feller, D. The role of databases in support of computational chemistry calculations. *J. Comp. Chem.* **1996**, *17*, 1571–1586. (b) Schuchardt, K.L.; Didier, B.T.; Elsethagen, T.; Sun, L.; Gurumoorthi, V.; Chase, J.; Li, J.; Windus, T. L. Basis Set Exchange: A Community Database for Computational Sciences. *J. Chem. Inf. Model.* **2007**, *47*, 1045-1052. (c) Pritchard, B. P.; Altarawy, D.; Didier, B.; Gibson, D. T.; Windus, T. L. A New Basis Set Exchange: An Open, Up-to-date Resource for the Molecular Sciences Community. *J. Chem. Inf. Model.* **2019**, *59*, 4814-4820.

(71) https://www.basissetexchange.org/ Accessed Aug 2020.